Title: **Erasable Hippocampal Neural Signatures Predict Memory Discrimination**

Authors: *Kinsky, Nathaniel R.[1,3,5], Orlin, Daniel J.[3,4,5], Ruesch, Evan A.[3], Diba, Kamran[1,2], *Ramirez, Steve[3]

Abstract

Memories involving the hippocampus can take several days to consolidate, challenging efforts to uncover the neuronal signatures underlying this process. Using calcium imaging in freely moving mice, we tracked the hippocampal dynamics underlying memory formation across a ten-day contextual fear conditioning (CFC) task. We found that cell turnover between the conditioning chamber and a neutral arena even *prior* to learning predicted the accuracy of subsequent memory recall the next day. Following learning, context-specific place field remapping correlated with memory performance. To causally test whether these hippocampal dynamics support memory consolidation, we induced amnesia in a group of mice by pharmacologically blocking protein synthesis immediately following learning. We found that halting protein synthesis following learning paradoxically accelerated cell turnover and also arrested learning-related remapping, paralleling the absence of remapping observed in untreated mice that exhibited poor memory expression. Finally, coordinated neural activity that emerged following learning was dependent on intact protein synthesis and predicted memory-related freezing behavior. We conclude that context-specific place field remapping and the development of coordinated ensemble activity require protein synthesis and underlie contextual fear memory consolidation.

Introduction

The process of memory consolidation requires protein synthesis following learning to produce stable long-term memories (Barondes & Cohen, 1968; Davis & Squire, 1984; Squire & Barondes, 1974). At the synaptic level, protein synthesis is necessary for the formation of late-phase but not early-phase long-term potentiation (LTP) in hippocampal (HPC) neurons (Frey & Morris, 1997; Huang et al., 1994; Nguyen et al., 1994). At the behavioral level, blocking protein synthesis following learning impairs long-term memory for hippocampus-dependent contextual fear conditioning (CFC) while leaving short term memory intact (Ryan et al., 2015; Schafe et al., 1999). These studies suggest that memory consolidation requires new proteins to reinforce learning-related connections which are potentiated during learning. Despite the evidence linking *in vitro* synaptic potentiation to memory consolidation, little is known about how protein synthesis *in vivo* influences the functional coding properties of neurons before, during, and after learning to support memory consolidation. Experience-dependent remapping of place fields in

[1]Department of Anesthesiology, University of Michigan Medical School, Ann Arbor, MI 48109, USA
[2]Neuroscience Graduate Program, University of Michigan, Ann Arbor, MI 48109, USA
[3]Center for Systems Neuroscience, Boston University, Boston, MA 02451, USA
[4]Neuroscience Graduate Program, Oregon Health & Science University, Portland, OR 97239, USA
[5]These authors contributed equally to this work
[*]Corresponding authors. Correspondence should be addressed to N.R.K (nkinsky@umich.edu) or S.R. (dvsteve@bu.edu)

the hippocampus, which requires NMDA receptor dependent-plasticity (Dupret et al., 2010), is thought to reflect learning-related reorganization of the hippocampal network (Bostock et al., 1991; Colgin et al., 2008). Therefore, to causally test the hypothesis that lasting, learning-related place-cell remapping (Muller & Kubie, 1987) is necessary for consolidation of a CFC memory (Moita et al., 2004; Wang et al., 2012) we combined *in vivo* calcium imaging in mice with systemic administration of the protein synthesis inhibitor, anisomycin, and tracked the evolution, remapping, and stabilization of HPC place fields during and after CFC. We further explored how between-animal variability in HPC dynamics *prior to learning* influenced memory recall accuracy. Finally, we leveraged the ability to record from large cell ensembles to investigate whether blocking protein synthesis disrupted the development of coordinated neural activity predictive of freezing behavior. Our results indicate that context-specific remapping and coordinated, freeze-predicting ensemble activity emerge in a protein-synthesis dependent manner following learning to support CFC memory consolidation.

Results

Hippocampal neural dynamics between arenas predicts memory specificity

Weeks prior to training, all mice received viral infusions of the genetically encoded calcium indicator GCaMP6f (Chen et al., 2013) in region CA1 of the dorsal hippocampus. Subsequently, following two days of pre-exposure ("Before" learning, days -2 and -1) to an operant chamber (shock arena) and an open field (neutral arena), mice received a mild foot-shock on day 0 (training), after which they were moved to their home cage and immediately given systemic injections of either anisomycin (ANI group) or vehicle (CTRL group). We then performed a test of short-term memory 4 hours later and three tests of long-term memory 1, 2, and 7 days following training (Figure 1A), each time by measuring freezing behavior. We titrated the shock level during training such that the mice froze significantly more in the shock arena relative to the neutral arena following learning while still exploring the majority of both arenas. We observed a range of freezing levels during the day 1 and 2 memory tests (Figure S1A) and sub-divided CTRL mice into two groups: Learners, who froze significantly more in the shock arena, and Non-Learners, who either showed generalized freezing or froze at low levels in both arenas (Figures 1B, 1G, Figure S1B). Learners exhibited reduced freezing on day 7, indicative of extinction (Figure 1B). All subsequent analyses related to long-term memory therefore utilized the day 1 and 2 recall sessions ("After" learning and consolidation). In contrast, mice in the ANI group exhibited no difference in freezing between arenas at any time point, indicating that blocking protein synthesis impaired context-specific fear memory (Figure 1C). Both the CTRL and ANI groups exhibited significant freezing in the shock arena during the 4 hour test (Figure 1D, Figure S1A), though we note that the behavior in the ANI group at this time point could arise from either contextual fear or non-specific aversive effects of anisomycin treatment (Figure S2) since these mice froze at high levels in both arenas.

We visualized the activity of pyramidal neurons in region CA1 of the dorsal hippocampus (Figure 1C) using a miniaturized epifluorescence microscope (Ghosh et al., 2011; Ziv et al., 2013). We identified a large number of neurons in each 10 minute session (n = 128 to 1216), extracted their corresponding calcium traces, and tracked them between sessions throughout the CFC task, which allowed us to determine the long-term evolution of the HPC neural code (Figure 1C,F). We next assessed behavioral expression of a CFC memory by calculating a behavioral discrimination index (DI_{beh}) to quantify how much each animal froze in the shock vs. neutral arenas. Negative DI values indicated higher freezing in the shock arena. Learners

exhibited negative DI_{beh} levels on days 1 and 2 that were significantly different from both Non-Learners (by definition) and from the ANI group as well (Figure 1G). We noticed that many neurons exhibited strong changes in mean event rate between arenas (Figure 1F) and calculated a neural discrimination index (DI_{neural}) to quantify the distinctiveness of neural activity

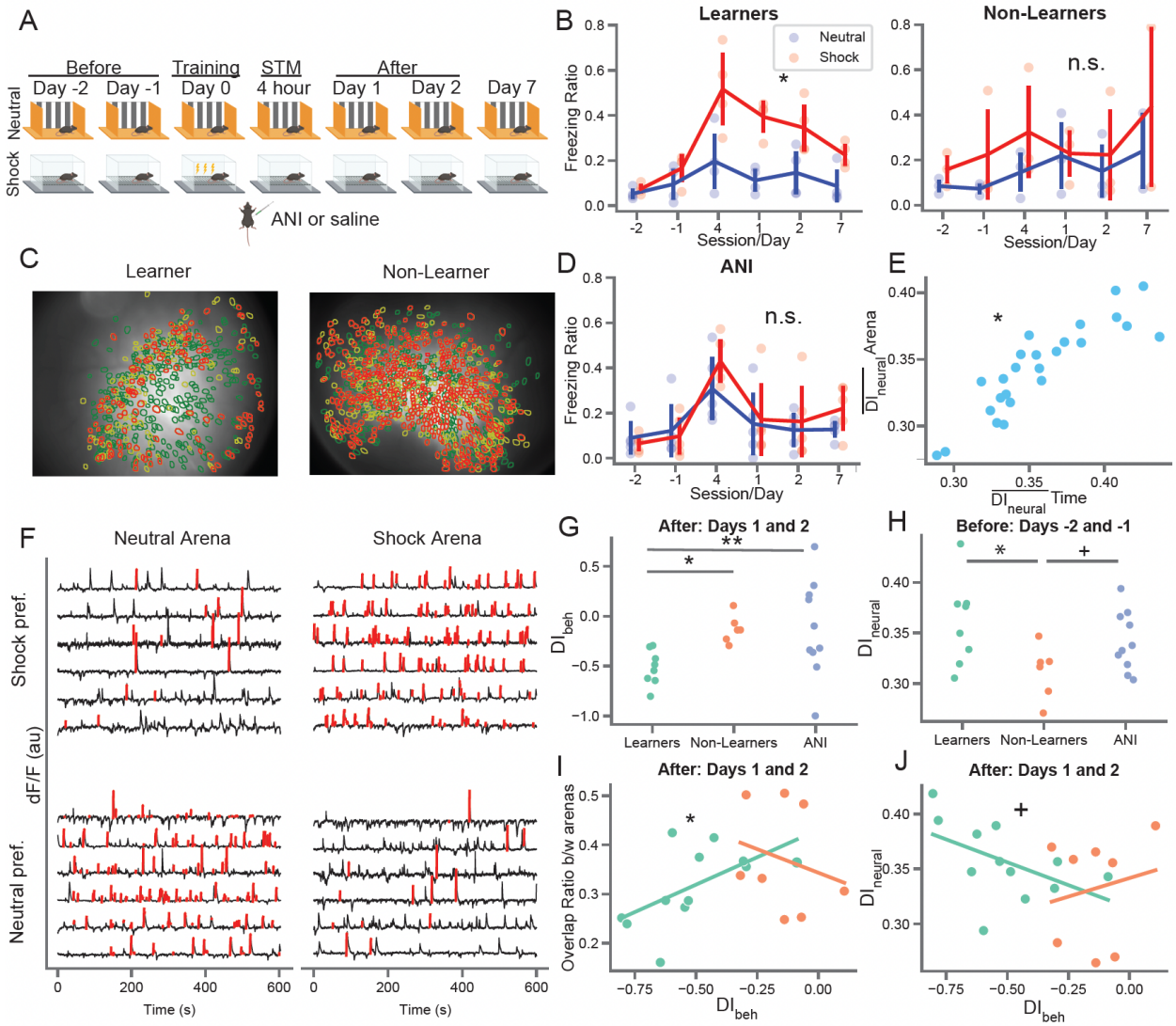

Figure 1: Neural discrimination between arenas predicts specificity of fear learning. A) Schematic of the behavioral paradigm. Mice freely explored two distinct arenas (neutral and shock) for 10 minutes each day. Mice underwent mild contextual fear conditioning on day 0 in the shock arena followed by immediate I.P. administration of anisomycin or vehicle in their home cage. Memory recall tests were conducted 4 hours and 1, 2, and 7 days post-shock. The time of each session is referenced to the shock session. **B)** (left) Learner (CTRL) mice freezing on all days. Red = shock arena, blue = neutral arena. *p=1.3e-0.5 shock **-** neutral freezing from days -2/-1 to days Ĺ one-sided t-test (n=4 mice). (right) Same but for Non-Learner (CTRL) mice (n=3 mice). **C)** (left) Neural overlap plots between neutral and shock arenas for an example Learner mouse on day -1, before shock. Green = cells active in the shock arena only, yellow = cells active in the neutral arena only, orange = cells active in both arenas. (right) Same for example Non-Learner on day -2 showing higher overlap of active cells between arenas. **D)** Same as B but for ANI group **E)** Mean neural discrimination between arenas (same day, days -2 to -1 and 1 to 2) vs. within arenas (same arena, days -2 and -1, days 1 and 2). *p=2.35e-8 (ρ=-0.56) Spearman correlation. **F)** Example calcium activity from the Learner mouse shown in C (left) for cells active in both arenas. Black = calcium trace, red = putative spiking activity during transient rises. Top row shows shock arena preferring cells, bottom row shows neutral arena preferring cells. **G)** Behavioral discrimination between arenas after shock (Days 1-2) shows formation of a specific fear memory for Learners only, by definition (positive = more freezing in neutral arena, negative = more freezing in shock arena, 0 = equal freezing in both arenas). *p=0.022, **p=0.00038 1-sided t-test **H)** Neural discrimination between arenas BEFORE shock indicates Learners formed more distinct representations of each arena prior to learning. Same conventions as F. *p=0.030, +p=0.059 two-sided t-test. **I)** Neural overlap between arenas correlates with specificity of fear memory on days 1-2 for Learners but not Non-Learners. *p=0.033 (ρ=0.61). **J)** Same as I) but plotting neural overlap vs. behavioral discrimination between arenas. +p=0.059 (ρ=-0.56) for Learners.

between arenas (0 = similar, 1 = distinct). Same-day neural discrimination between arenas correlated strongly with across-day neural discrimination in the same arena (Figure 1E, Figure S1C). This indicates that mice exhibit natural variability in neural discrimination which is invariant between different arenas and across time. Interestingly, we noticed that DI_{neural} was significantly higher for Learners vs. Non-Learners in the sessions *prior to* the shock (Figure 1H), indicating that inherent differences in neural discrimination influence how well mice learn the CFC task. In other words, poorer neural discrimination between arenas was predictive of impaired CFC learning.

Previous work has demonstrated that higher overlap between HPC neurons active in two distinct arenas correlates with increased generalization or linking of a contextual fear memory across arenas (Cai et al., 2016). Accordingly, we hypothesized that the distinctiveness of the HPC neural code between arenas would predict how much mice froze in the neutral arena. We therefore utilized a regression analysis to determine if neural discrimination during memory recall *after shock* likewise correlated with memory discrimination. We utilized two metrics to quantify the distinctiveness of the HPC neural code between arenas: 1) the overlap ratio of neurons active in both arenas divided by the total number of cells active in either arena, which accounts for cells that may be silent in one of the arenas, and 2) the aforementioned DI_{neural} metric, which is based on the cells that are active in both arenas. We found that overlap ratio was significantly correlated with DI_{beh} for Learners, but not for Non-Learners, on days 1-2 (Figure 1I); likewise, the correlation between DI_{beh} and DI_{neural} approached significance for Learners but not for Non-Learners on days 1-2 (Cai et al., 2016; Figure 1J). Together, our results indicate that mice with segregated experiences in the HPC neural code were more capable of forming discrete long-term memories and that the distinctiveness of HPC calcium activity predicts the specificity of memory for CFC.

Blocking protein synthesis disrupts persistent neural activity following learning and arrests learning-related place field remapping

Next, we probed how arresting protein synthesis impacted HPC dynamics. We hypothesized that, by preventing plasticity, ANI administration would slow or stop the normal rate of cell turnover observed across days (Figure 2A). Surprisingly, we found that ANI administration rapidly accelerated the turnover in which cells are active at any given time. Cell turnover was indicated by lower overlap of active cells from experiment start to the 4 hour session in the ANI group compared to the CTRL group (Figure 2A-C). Increased turnover in the ANI group appeared to be driven by a sharp decrease in the number of active neurons at the 4 hour session following administration of anisomycin, despite these mice displaying comparable levels of freezing to CTRL group mice at this time point (Figure 2D). This accelerated turnover in cells was temporary and was followed by a decrease in the cell turnover rate from the 4 hour to day 1 session for the ANI compared to the CTRL group (Figure 2B-C). Importantly, we observed no difference in the mean height of calcium transients (a measure of signal-to-noise ratio) for neurons active before, during, or after ANI administration, indicating that the observed decrease in the number of active neurons was not due to differences in Ca2+ levels or depletion of the GCaMP protein (Figure S7D-E). To confirm that this decrease in activity was not due to suppression of network activities, such as those reported for intracranial infusions of protein synthesis inhibitors in anesthetized or immobile rodents (Barondes & Cohen, 1966; Sharma et al., 2012), we performed extracellular recordings in a freely moving rat implanted with a linear probe in the CA1 region of the hippocampus following administration of anisomycin. We

observed preserved theta activity, theta modulation of spiking, and robust sharp wave ripple activity for up to 5 hours following anisomycin administration (Figure S7A-C). These observations therefore indicate that blocking protein synthesis following learning does not abolish all neuronal activity but instead reduces the number of active neurons, which may be those specifically involved in learning.

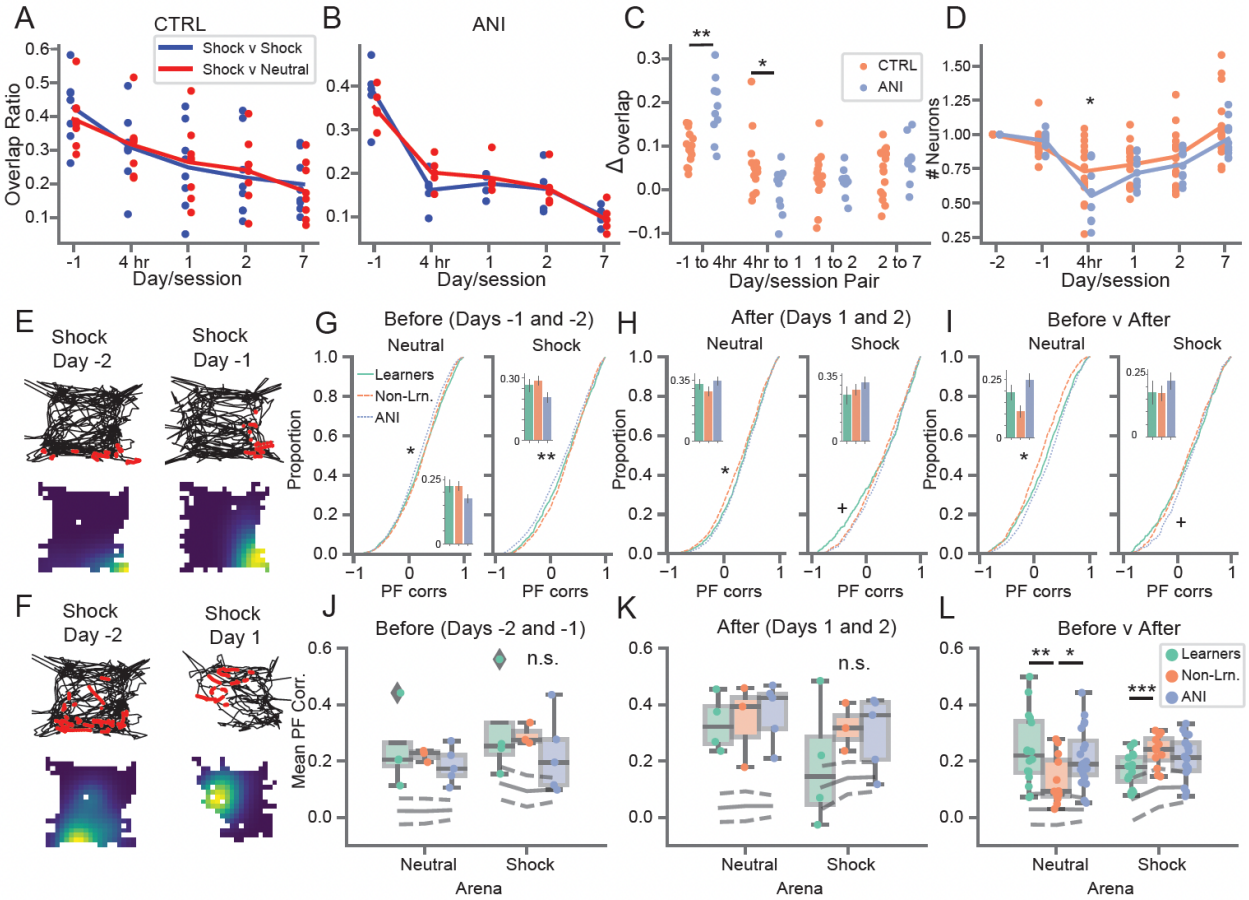

Figure 2: Anisomycin accelerates cell turnover and stifles learning-related place field remapping A) Cell overlap ratio with Day -2 session, CTRL group. Blue = within shock arena, red = shock v. neutral arena. **B)** Same as A) but for ANI group. **C)** Change in overlap ratios from a and b. *p=0.028, **p=0.00024 two-sided t-test. **D)** Number of active neurons observed each day, normalized to day -1. *p=0.039 two-sided t-test. **E)** Stable place field. (top) Example mouse trajectory (black) with calcium activity (red) overlaid for the same cell from day -2 to -1 in shock arena, (bottom) occupancy normalized rate maps for the same cells. **F)** Remapping place field. Same as E) but for a different cell that remaps from day -2 to day 1 in the shock arena. **G)** Place field correlations for all mice before shock (Days -2 and -1). *p<0.0032 Learners vs ANI and Non-Learners vs ANI, **p=1.9e-6 Non-Learners vs ANI, k-s test after Bonferroni correction. Inset = mean +/- 95% CI. **H)** Same as G) but for days after shock. *p=0.045 Learners vs Non-Learners and p=0.0059 Non-Learners vs ANI, +p=0.1 Learners vs ANI. **I)** Same as G) but to assess learning-related remapping from before to after shock. *p=0.00021 Learners vs Non-Learners and p=3.4e-11 Non-Learners vs ANI, +p=0.12 Learners vs ANI. **J)** Place field correlations before shock broken down by mouse. **K)** Same as J) but for sessions after shock. **L)** Same as J) but from before to after shock. p=0.002 mixed ANOVA, group x arena interaction. *p=0.025 Non-Learners vs ANI, **p=0.013 Learners vs Non-Learners, ***p=0.034 Learners vs ANI, post-hoc pairwise t-test after Bonferroni correction. Boxplots denote median and 1st/3rd quartiles, whiskers = 1.5 x interquartile range, gray solid/dashed line indicates mean +/- 95% CI for shuffled distribution.

We next hypothesized that arresting protein synthesis, which disrupts the permanence of newly formed place fields (Agnihotri et al., 2004), would likewise impair the long-term stability of CFC-related remapping (Moita et al., 2004; Wang et al., 2012). We therefore assessed place field remapping within and across epochs by correlating event rate maps for all neurons active between two sessions (Figure 2E-F) following administration of anisomycin, compared with saline. We noticed that place fields recorded in the Learners group exhibited very low across-session correlations in the neutral arena throughout the experiment (Figure S3), which could

141 indicate remapping. However, in a separate study, we observed what appeared to be
142 remapping between two recording sessions, but which was actually a coherent rotation of all
143 place fields around a singular point (Kinsky et al., 2018), indicative of confusion in an animal's
144 axis of orientation, such as between west and north (Keinath et al., 2017).

145 Importantly, such angular disorientation does not impair the ability of mice to identify specific
146 places (Julian et al., 2015), and between-cell firing relationships are maintained during coherent
147 rotations whereas they are scrambled following remapping. Coherent rotations match the
148 geometry of the environment, e.g. producing rotations in 60 degree increments in a triangle
149 versus 90 degrees in square environments such as our neutral and shock arenas.

150 Therefore, to ensure we were not mistaking coherent rotations for remapping, we rotated all
151 place field maps from each session in 90 degree increments and used only the orientation that
152 produced the highest correlation between sessions. We found generally higher correlations
153 compared to using non-rotated maps (Figure 2G-H, J-K vs. Figure S3F-G), confirming that
154 coherent rotations occurred in many recording sessions. In particular, place field correlations
155 were high both before learning and after consolidation (Figure 2J-K), though Learner
156 correlations trended toward lower stability after shock (Figure 2H,K) which could indicate
157 extinction. We then compared place fields from before (Days -2 and -1) to after (Days 1 and 2)
158 shock/learning to assess learning-related remapping. In agreement with previous studies (Moita
159 et al., 2004; Wang et al., 2012), Learner place fields remapped, as indicated by lower
160 correlations in the shock arena compared to the other groups (Figure 2I,L). Interestingly,
161 compared to the other groups, Non-Learners exhibited lower place map correlations in the
162 neutral arena, indicating paradoxically stable place fields in the shock arena but remapping in
163 the neutral arena (Figure 2I,L). If learning causes remapping, this double dissociation indicates
164 that Non-Learner memory deficits might result from improperly associating the neutral arena
165 with shock. In contrast, the place maps of mice in the ANI group displayed high correlations in
166 all arenas, including after learning. This deficit in remapping following anisomycin therefore
167 indicates that protein synthesis is required to stabilize the set of place fields which emerge
168 following learning to support memory consolidation. Overall, these observations indicate that
169 remapping is necessary for the creation of context-specific memories and that a lack of
170 remapping, or improperly remapping, may underlie the memory deficits observed in Non-
171 Learners and in the ANI group.

172 **Coordinated freeze-predictive neural activity emerges following consolidation**

173 In addition to the spatial code, hippocampal neural activity can also reflect non-spatial variables
174 in a task (McKenzie et al., 2014; Muzzio et al., 2009; Wood et al., 1999). We noticed that, in line
175 with recent studies (Lee & Han, 2022; Schuette et al., 2020), many hippocampal neurons
176 reliably produced calcium transients around the time that mice froze (Figure 3A-B, D-F and
177 S6A-C). Examining the +/- 4 seconds around freezing events for Days 1-2 (after learning)
178 revealed that population-level neural activity peaked in the 2 seconds prior to freezing for control
179 mice compared to the ANI group (Figure 3C). This pre-freeze increase in activity for the CTRL
180 vs. the ANI group was not present before learning or at the 4 hour session (Figure S6L-M). After
181 learning, neurons with significant peri-freeze tuning tiled the entire +/- 4 seconds around freeze
182 onset (Figure 3G). However, the average peak timing of cells with significant peri-freeze activity
183 shift shifted to significantly early time points for Learners vs. Non-Learners and ANI mice after
184 learning (Figure 3H) with ~70% of cells active before freeze onset. We observed similar

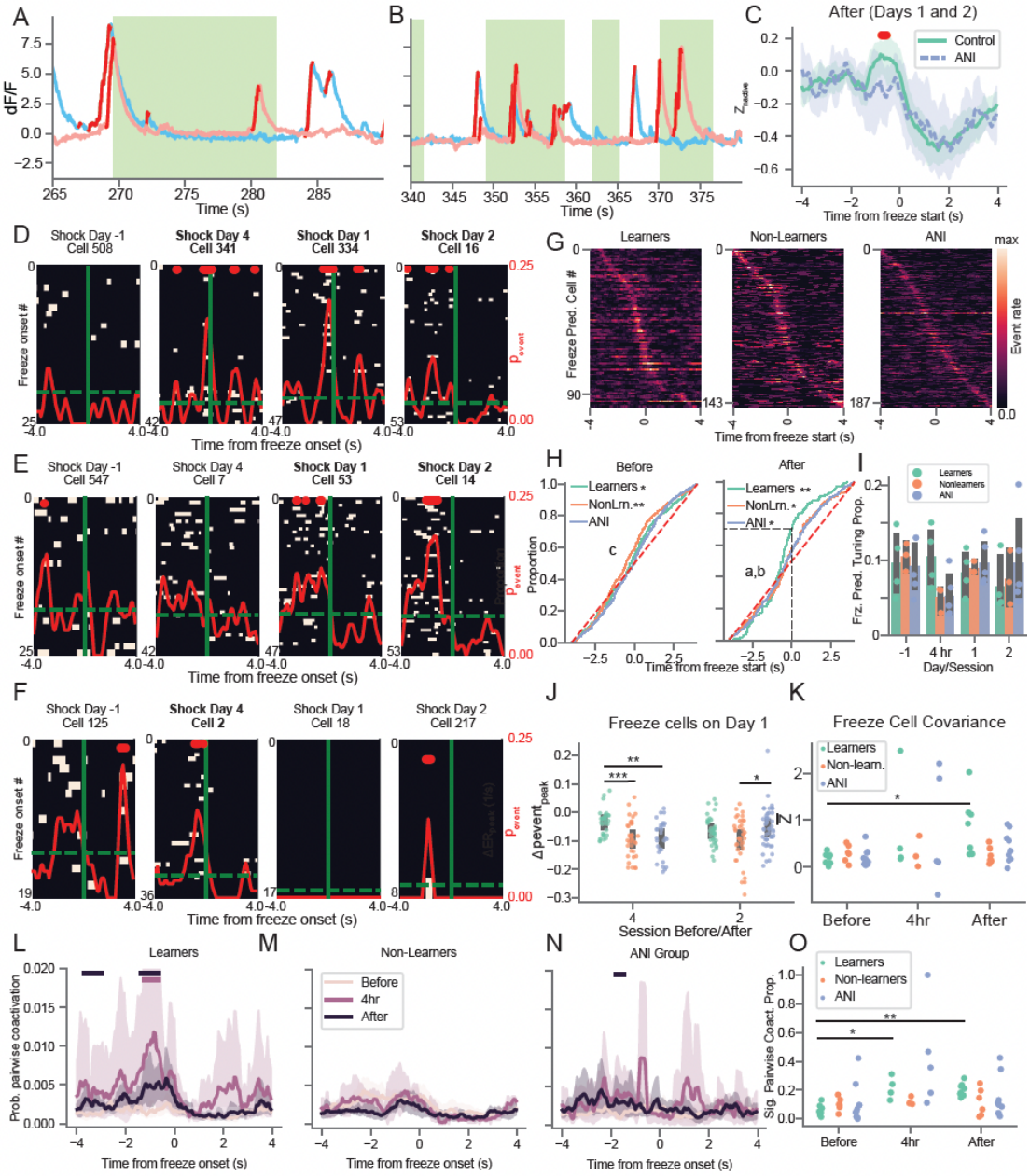

Figure 3: ANI administration suppresses the development of coordinated freeze-predicting neural activity. A) and B) Example traces from two freeze-predicting cells which exhibit coordinated activity prior to freezing event during the day 1 memory recall session in the shock arena. Red = putative spiking activity, pink = cell shown in C, blue = cell shown in E. **C)** After learning (Days 1 and 2), z-scored population level calcium activity peaks between 0 and 2 seconds prior to freezing for CTRL relative to the ANI group. Line/shading = mean +/- 95% CI. Red: bins with $p < 0.05$, independent t-test (two-sided). **D) and E)** Example Learner freeze-predicting cells identified during the 4 hour (D) or day 1 (E) memory test tracked across sessions. Peri-event calcium activity rasters are centered on freeze onset time (solid green). Dashed green = baseline calcium event probability, red solid = peri-freeze calcium event probability, bins with $p<0.01$ (circular permutation test) noted with red bars at top. D/E corresponds to pink/blue cells shown in A-B. Bold = session with significant freeze-tuning. **F)** Same as D and E but for ANI mouse immobility-predicting cell identified during the 4 hour session. **G)** Peri-freeze calcium event probability for all freeze-predicting cells detected for each group after learning (Days 1-2), sorted by time of peak activation. **H) (left)** Cumulative distribution of peak peri-freeze activation times before learning. *p=0.49, **p=1e-5 two-sided Wilcoxon rank-sum test , c: p=0.005 Non-Learners v. ANI, 1-sided Mann-Whitney U-test. **(right)** same as left but for after learning. *$p < 0.022$, **p=2e-7 two-sided Wilcoxon rank-sum test. a: p=0.022 Learners v. Non-Learners, b: p=0.029 Learners v. ANI 1-sided Mann-Whitney U-test. **I)** Proportion of freeze-predicting cells detected each day across all groups. Green = freezing epochs. **J)** Change in peak peri-freeze calcium event probability for all freeze-predicting cells detected during the 1 day session. $p < 0.02$ 1-way ANOVA each day separately, *p=0.02, **p=0.001, ***p=0.0006 post-hoc Mann-Whiney U-test. **K)** Freeze-predicting cells exhibit increased peri-freeze covariance for Learners but not Non-Learners or ANI group mice. Mean covariance of freeze-tuned cells from each session shown. p=0.047 two-way ANOVA. *p=0.001 post-hoc pairwise t-test (two-sided) after Bonferroni correction. **L-N)** Pairwise coactivation probability of all freeze-predicting cells during Before, 4 hour, and After sessions. Maroon/Black bars at top indicate significant increases in coactivation at 4 hour / After time points compared to before, $p< 0.01$ 1-sided Mann-Whitney U-test. **O)** Proportion of freeze/immobility-predictive cells with significant pairwise coactivation compared to chance (trial shuffle). p=0.02 two-way ANOVA. *p=0.036, **p=0.0014 post-hoc pairwise Mann-Whitney U-test after Bonferroni correction. Line/shading = mean +/- 95% CI.

185

proportions of peri-freeze tuned cells across all groups and recording sessions, even before CFC (Figure 3I, Figure S6D). However, following CFC we noticed that peri-freeze tuned cells appeared to activate more reliably around, and particularly before, freezing epochs for Learners compared to similar immobility epochs in Non-Learners and in the ANI group (Figure 3D-E vs. Figure 3F and Figure S6B-C). We therefore refer to these neurons as freeze-predictive cells, noting that predictive activity is particularly pronounced in Learners compared to Non-Learners and the ANI group.

To quantify changes in the reliability of freeze-predictive turning within cells, we tracked the peak, peri-freeze calcium event probability of each freeze cell backwards and forwards in time from the Day 1 recall session, after putative memory consolidation had occurred. We found that freeze-predictive cells exhibited much higher tuning stability spanning from the 4 hour recall to the day 2 recall sessions in Learners than did these cells in other groups (Figure 3J). This indicates that in Learners, reliable freeze-predictive tuning began to emerge between 4 hours and 1 day following learning and was maintained thereafter (see Figure 3E for exemplar cell). In contrast, peri-immobility activities in mice from the ANI group and in Non-Learners were more transient and unreliable during this time span.

Lastly, we investigated whether the higher reliability of freeze-predicting cells in Learners was related to increased co-activity (see Figure 3A-B) in this neuronal subpopulation. Peri-freeze cell covariance increased significantly from before to after learning for Learners but not for Non-Learners nor for mice treated with ANI (Figure 3K). A similar increase in covariance for Learners was also observed across all cells in the shock arena (Figure S6G, I) but not in the neutral arena (Figure S6E), indicating that CFC learning enhances ensemble-level neural activity particularly prior to freezing. The ANI group also displayed increased covariance between all cells at the 4 hour session, but not at subsequent time points for which consolidation has been shown to depend on protein synthesis. We observed a similar trend in freeze-predicting cell covariance when we downsampled the number of freezing events following learning to match that on days -2 and -1 (Figure S6H). For freeze-predicting cells, but not all cells in general, the increased covariance was driven by peri-freeze neural activity (Figure S6F, I).

In these analyses we compared freeze-predictive cells identified independently on each day of the experiment. We next performed additional analyzes focused on the same set of freeze-predictive cells conditioned on their activity during the Day 1 recall test immediately after putative memory consolidation was finalized. Freeze-predicting cells identified on the 1 day recall session displayed increased covariance following CFC in Learners but not in Non-Learners or in the ANI group (Figure S6J). However, these cells did not exhibit increased covariance during the previous day's 4 hour session, indicating that even though freeze-predictive activity begins to emerge immediately following learning, functional cell connections continue to reorganize up to one day later to form coordinated ensembles. Next, we examined the time-course of coordinated activity by calculating pairwise coactivation of neurons +/- 4 seconds from freeze onset. We found that pairwise coactivation increased significantly from 0-2 seconds prior to freezing the 4 hour and after learning sessions for Learners but not for Non-Learners or for ANI group mice. Finally, to account for the overall increase in population-level activity prior to freezing (Figure 3C), we calculated chance level pairwise coactivation by shuffling the order of freeze onsets for one cell in each pair 100 times and calculating the probability that the actual pairwise chance exceeded shuffle for each bin. We found that the proportion of freeze-predicting cells with significant coactivation (> 3 consecutive bins with

231 coactivity exceeding 95% of shuffles) increased for Learners, but not Learners or ANI group
232 mice, from before learning to the 4 hour recall session and before learning to after learning
233 recall sessions (Figure 3O). These results demonstrate that freeze-predictive tuning emerges
234 following learning and continues to take shape in the ensuing hours until it stabilizes one day
235 later. Importantly, the coordination of these freeze-predictive cells into neuronal ensembles
236 requires protein synthesis, and their failure to coactivate does not occur under memory
237 consolidation failures.

238 Discussion

239 The results of our study provide evidence that HPC spatial representations support contextual
240 memory formation and consolidation. We found that inherent neural variability in HPC neuron
241 turnover between arenas *prior to learning* impacted the accuracy of subsequent contextual fear
242 memory recall. Conversely, we found that the similarity of neural representations *after*
243 *consolidation* correlated with the generalization of the fear memory recall to the neutral arena.
244 Based on these observations, we propose that the ability of the HPC to form distinct
245 representations of two arenas despite overlapping contextual qualities allows for the formation
246 of discrete contextual memories that could underlie why some mice learn while others do not
247 (Cai et al., 2016). One mechanism for distinguishing experiences that occur close together is
248 representational drift: the observation that neural activity continually changes despite stable
249 behavior and external stimuli (Kinsky et al., 2020; Levy et al., 2021; Mankin et al., 2012; Ziv et
250 al., 2013). Drift is hypothesized to provide a mechanism for "timestamping" events and facilitate
251 linking of experiences that occur close together in time or separating experiences which occur
252 further apart in time (Geva et al., 2023; Rubin et al., 2015). Under this framework, slower drift
253 (as measured by neuron turnover) between sessions/arenas decreases the ability of an animal
254 to separate experiences close in time at the neural level, which could in turn impair associative
255 learning, or alternatively, enhance memory linking (Cai et al., 2016). Our finding that animals
256 with high levels of drift form more specific CFC memories provide strong support for this
257 viewpoint.

258 We next probed how protein-synthesis influenced learning-related hippocampal dynamics
259 following CFC. We saw that anisomycin acutely suppressed the number of active cells
260 immediately following learning. In addition to this suppression, anisomycin's amnestic effects
261 coincided with a reduction in learning-related remapping, effectively halting HPC contextual
262 representations in their prior state. This paralleled the absence of remapping in the shock arena
263 for Non-Learners, providing strong evidence for the persistence of remapping as a mechanism
264 underlying spatial memory consolidation. Given that remapping *was* observed in Learners
265 during this time window, we speculate that arresting protein synthesis temporarily blocked the
266 formation of new place-fields in the subset of cells that would otherwise undergo remapping
267 following CFC. By this conjecture, place-cell activity following ANI was reduced because of
268 impairment in the formation and strengthening of new neuronal connections. This idea is
269 resonant with the notion that more excitable/active neurons are preferentially involved in
270 memory trace formation (Rashid et al., 2016; Sweis et al., 2021). While reduced activity could
271 also potentially result from non-specific effects of ANI, or the blockage of constitutive protein
272 translation (Scavuzzo et al., 2019), our study does not support this view; we did not observe a
273 widespread shutdown of neural activity as both theta oscillations and sharp-wave ripples were
274 intact in ANI-treated mice. Surprisingly, remapping occurred in untreated mice that exhibited
275 poor memory recall (Non-Learners); however, this remapping was limited to the neutral arena.

This indicates that ANI induced memory failures and poor learning do not necessarily share the same mechanism. ANI impairs memory by preventing learning-related plasticity which stifles remapping, while poor learning can occur when the shock is improperly associated with the neutral arena. Overall, our findings support the view that the long-term stability of learning-related remapping requires protein synthesis and underlies CFC memory consolidation.

Lastly, we found that a subset of hippocampal cells reliably activated near freezing events during fear memory recall, consistent with a previous report (Schuette et al., 2020). These cells activities were particularly heightened 1-2 seconds prior to freezing epochs in animals which exhibited a strong, specific CFC memory but not in the ANI group or untreated mice which exhibited poor memory. The predictive nature of these cells distinguishes them from previously reported immobility cells which occur primarily in CA2 but also in CA1 (Kay et al., 2016). We further found that freeze-predictive cells organized into reliable, co-active neuronal ensembles following learning (Lee & Han, 2022). Importantly, the covariance of all cells increased incrementally for both ANI and Learner groups at the 4 hour recall session, a time point at which protein synthesis is not considered to be required for the induction of (early-phase) long-term potentiation *in vitro* (Frey & Morris, 1997; Nguyen et al., 1994). However, at later time points, when protein synthesis *is* indeed found to be required to maintain (late-phase) long-term potentiation (Frey et al., 1993; Nguyen et al., 1994), between-cell covariance remained high for Learners only (Figure S6G, I). Therefore, in addition to maintaining learning-related synaptic changes over hours to days, protein synthesis might also be instrumental for producing coordinated firing of large ensembles of neurons.

The synchronous bursts of neuron ensembles we observed prior to freezing may provide a neuronal basis for memory recall. For example, they could indicate the activation of sharp-wave ripples (SWRs): transient, high frequency oscillations observable in the hippocamp local field potential which can facilitate transmitting information throughout the cortex. SWRs are primarily observed during periods of awake immobility and sleep and are hypothesized support memory consolidation and planning through reactivation of neuronal activity patterns observed during learning and active exploration (Buzsáki, 2015). However, SWRs can also occur during periods of movement; these exploratory SWRs (eSWRs) are posited to strengthen connections between place cells for reactivation and subsequent stabilization during sleep (O'Neill et al., 2006). In line with this view, synchronous neuronal activation during eSWRs could strengthen connections between freeze-predicting cells and stabilize their activity patterns to guide future memory recall. Alternatively, coordinated activation of these cells could cooccur with other prominent hippocampal oscillations such as theta or gamma (Colgin, 2016). Whether it occurs with SWRs, theta, or gamma, coincident firing of freeze-predictive ensembles could be important for guiding memory recall. In line with this idea, one study demonstrated that synchronous optogenetic stimulation of engram neurons tagged during learning could artificially reactivate a fear memory even when normal long-term recall of the fear memory was hindered by arresting protein synthesis after learning, suggesting that a memory trace still resided in the network (Ryan et al., 2015). Our findings provide a parsimonious explanation for this previous result by demonstrating that anisomycin halts the co-activation of freeze-predictive cells, weakening the capacity of these neurons to transmit behavior-related information to downstream regions through coincident firing (Lisman, 1997) and impairing their ability to trigger memory recall (Ryan & Frankland, 2022).

Overall, our results provide a bridge between the neuronal activities that underly memory formation and the protein signaling events that are critical for plastic modification of synapses, indicating that protein synthesis is necessary for the formation of new stable spatial representations of an aversive context following learning and for producing coordinated activity of freeze-predictive neurons.

Acknowledgments: First and foremost, we would like to thank Howard Eichenbaum who helped conceive and design this study before his unfortunate passing in 2017. We would also like to thank Sam McKenzie for his help during early experimental design. We would like to thank Michael Hasselmo and Ian Davison for their support and feedback while performing the recordings for this study. Next, we thank Sam Levy, Dave Sullivan, and Will Mau for their assistance in all phases of calcium imaging throughout. We would like to thank Zach Pennington for valuable feedback concerning anisomycin preparation and administration, and Denise Cai and Lucas Carstensen for analysis suggestions. We would like to thank Pho Hale, Rachel Wahlberg, and Utku Kaya for feedback on the manuscript. We would like to acknowledge the GENIE Program, specifically Vivek Jayaraman, PhD, Douglas S. Kim, PhD, Loren L. Looger, PhD, Karel Svoboda, PhD from the GENIE Project, Janelia Research Campus, Howard Hughes Medical Institute, for providing the GCaMP6f virus. Finally, we would like to acknowledge Inscopix, Inc. for making single-photon calcium imaging miniscopes widely available, and specifically Lara Cardy and Vardhan Dani for all their technical support throughout the experiment. This work was supported by NIH Grants R01 MH052090, R01 MH051570, R01MH117964, NIH NRSA Fellowship 1F32NS117732-01, NIH Early Independence Award DP5 OD023106-01, an NIH Transformative R01 Award, a Young Investigator Grant from the Brain and Behavior Research Foundation, a Ludwig Family Foundation grant, and the McKnight Foundation Memory and Cognitive Disorders award, and Boston University's Neurophotonics Center.

Author Contributions

Conceptualization: N.R.K with the help of Howard Eichenbaum; Methodolgy: N.R.K; Software: N.R.K., E.A.R; Validation: N.R.K; Formal Analysis: N.R.K, D.J.O., E.A.R; Investigation: N.R.K., D.J.O., E.A.R.; Data Curation: N.R.K., D.J.O., E.A.R.; Writing – original draft preparation: N.R.K.; Writing – review and editing; N.R.K, D.J.O, E.A.R., K.D., S.R.; Visualization: N.R.K.; Project Administration; N.R.K, S.R.; Funding Acquisition: N.R.K., K.D., S.R.

Competing Interests

The authors declare no competing interests.

Materials & Correspondence

All requests for materials and correspondence should be directed to Nat Kinsky (nkinsky@umich.edu) or Steve Ramirez (dvsteve@bu.edu).

References

Agnihotri, N. T., Hawkins, R. D., Kandel, E. R., & Kentros, C. G. (2004). The long-term stability of new hippocampal place fields requires new protein synthesis. *Proceedings of the National Academy of Sciences*, *101*(10), 3656–3661. https://doi.org/10.1073/pnas.0400385101

Barondes, S. H., & Cohen, H. D. (1966). Puromycin Effect on Successive Phases of Memory Storage. *Science*, *151*(3710), 594–595. https://doi.org/10.1126/science.151.3710.594

Barondes, S. H., & Cohen, H. D. (1968). Memory impairment after subcutaneous injection of acetoxycycloheximide. *Science (New York, N.Y.)*, *160*(3827), 556–557. http://www.ncbi.nlm.nih.gov/pubmed/5689416

Bostock, E., Muller, R. U., & Kubie, J. L. (1991). Experience-dependent modifications of hippocampal place cell firing. *Hippocampus*, *1*(2), 193–205. https://doi.org/10.1002/hipo.450010207

Buzsáki, G. (2015). Hippocampal sharp wave-ripple: A cognitive biomarker for episodic memory and planning. *Hippocampus*, *25*(10), 1073–1188. https://doi.org/10.1002/hipo.22488

Cai, D. J., Aharoni, D., Shuman, T., Shobe, J., Biane, J., Lou, J., Kim, I., Baumgaertel, K., Levenstain, A., Tuszynski, M., Mayford, M., & Silva, A. J. (2016). A shared neural ensemble links distinct contextual memories encoded close in time. *Nature*, *534*, 115–118. https://doi.org/10.1038/nature17955

Chen, T.-W., Wardill, T. J., Sun, Y., Pulver, S. R., Renninger, S. L., Baohan, A., Schreiter, E. R., Kerr, R. a, Orger, M. B., Jayaraman, V., Looger, L. L., Svoboda, K., & Kim, D. S. (2013). Ultrasensitive fluorescent proteins for imaging neuronal activity. *Nature*, *499*(7458), 295–300. https://doi.org/10.1038/nature12354

Colgin, L. L. (2016). Rhythms of the hippocampal network. *Nature Reviews Neuroscience*, *17*(4), 239–249. https://doi.org/10.1038/nrn.2016.21

Colgin, L. L., Moser, E. I., & Moser, M.-B. (2008). Understanding memory through hippocampal remapping. *Trends in Neurosciences*, *31*(9), 469–477. https://doi.org/10.1016/j.tins.2008.06.008

Davis, H. P., & Squire, L. R. (1984). Protein synthesis and memory: A review. *Psychological Bulletin*, *96*(3), 518–559. https://doi.org/10.1037/0033-2909.96.3.518

Dupret, D., O'Neill, J., Pleydell-Bouverie, B., & Csicsvari, J. (2010). The reorganization and reactivation of hippocampal maps predict spatial memory performance. *Nature Neuroscience*, *13*(8), 995–1002. https://doi.org/10.1038/nn.2599

Frey, U., Huang, Y.-Y., & Kandel, E. R. (1993). Effects of cAMP Simulate a Late Stage of LTP in Hippocampal CA1 Neurons. *Science*, *260*(5114), 1661–1664. https://doi.org/10.1126/science.8389057

Frey, U., & Morris, R. G. M. (1997). Synaptic tagging and long-term potentiation. *Nature*, *385*(6616), 533–536. https://doi.org/10.1038/385533a0

Geva, N., Deitch, D., Rubin, A., & Ziv, Y. (2023). Time and experience differentially affect distinct aspects of hippocampal representational drift. *Neuron*, *111*(15), 2357-2366.e5. https://doi.org/10.1016/j.neuron.2023.05.005

Ghosh, K. K., Burns, L. D., Cocker, E. D., Nimmerjahn, A., Ziv, Y., Gamal, A. El, & Schnitzer, M. J. (2011). Miniaturized integration of a fluorescence microscope. *Nature Methods*, *8*(10), 871–878. https://doi.org/10.1038/nmeth.1694

Huang, Y. Y., Li, X. C., & Kandel, E. R. (1994). cAMP contributes to mossy fiber LTP by initiating both a covalently mediated early phase and macromolecular synthesis-dependent late phase. *Cell*, *79*(1), 69–79. https://doi.org/10.1016/0092-8674(94)90401-4

Julian, J. B., Keinath, A. T., Muzzio, I. A., & Epstein, R. A. (2015). Place recognition and heading retrieval are mediated by dissociable cognitive systems in mice. *Proceedings of the National Academy of Sciences*, *112*(20), 6503–6508. https://doi.org/10.1073/pnas.1424194112

Kay, K., Sosa, M., Chung, J., Karlsson, M. P., Larkin, M., Grossrubatscher, I., & Frank, L. M. (2016). A hippocampal network for spatial coding during immobility. *Nature*, *531*, 185–190. https://doi.org/10.1038/nature17144

Keinath, A. T., Julian, J. B., Epstein, R. A., & Muzzio, I. A. (2017). Environmental Geometry Aligns the Hippocampal Map during Spatial Reorientation. *Current Biology*, *27*(3). https://doi.org/http://dx.doi.org/10.1016/j.cub.2016.11.046

Kinsky, N. R., Mau, W., Sullivan, D. W., Levy, S. J., Ruesch, E. A., & Hasselmo, M. E. (2020). Trajectory-modulated hippocampal neurons persist throughout memory-guided navigation. *Nature Communications*, 1–14. https://doi.org/10.1038/s41467-020-16226-4

Kinsky, N. R., Sullivan, D. W., Mau, W., Hasselmo, M. E., & Eichenbaum, H. B. (2018). Hippocampal Place Fields Maintain a Coherent and Flexible Map across Long Timescales. *Current Biology*, *28*(22), 1–11. https://doi.org/10.1016/J.CUB.2018.09.037

Lee, H.-S., & Han, J.-H. (2022). Activity patterns of individual neurons and ensembles correlated with retrieval of a contextual memory in the dorsal CA1 of mouse hippocampus. *The Journal of Neuroscience*, *43*(1), JN-RM-1407-22. https://doi.org/10.1523/jneurosci.1407-22.2022

Levy, S. J., Kinsky, N. R., Mau, W., Sullivan, D. W., & Hasselmo, M. E. (2021). Hippocampal spatial memory representations in mice are heterogeneously stable. *Hippocampus*, *31*(3), 244–260. https://doi.org/10.1002/hipo.23272

Lisman, J. E. (1997). Bursts as a unit of neural information: Making unreliable synapses reliable. *Trends in Neurosciences*, *20*(1), 38–43. https://doi.org/10.1016/S0166-2236(96)10070-9

Mankin, E. A., Sparks, F. T., Slayyeh, B., Sutherland, R. J., Leutgeb, S., & Leutgeb, J. K. (2012). Neuronal code for extended time in the hippocampus. *Proceedings of the National Academy of Sciences*, *109*(47), 19462–19467. https://doi.org/10.1073/pnas.1214107109

Mau, W., Sullivan, D. W., Kinsky, N. R., Hasselmo, M. E., Howard, M. W., & Eichenbaum, H. B. (2018). The Same Hippocampal CA1 Population Simultaneously Codes Temporal Information over Multiple Timescales. *Current Biology*, *28*(10), 1499-1508.e4. https://doi.org/10.1016/j.cub.2018.03.051

McKenzie, S., Frank, A. J., Kinsky, N. R., Porter, B., Rivière, P. D., & Eichenbaum, H. B. (2014). Hippocampal representation of related and opposing memories develop within distinct, hierarchically organized neural schemas. *Neuron*, *83*(1), 202–215. https://doi.org/10.1016/j.neuron.2014.05.019

Moita, M. A. P., Rosis, S., Zhou, Y., LeDoux, J. E., & Blair, H. T. (2004). Putting Fear in Its Place: Remapping of Hippocampal Place Cells during Fear Conditioning. *Journal of Neuroscience*, *24*(31), 7015–7023. https://doi.org/10.1523/JNEUROSCI.5492-03.2004

Muir, D. R., & Kampa, B. M. (2015). FocusStack and StimServer: a new open source MATLAB toolchain for visual stimulation and analysis of two-photon calcium neuronal imaging data. *Frontiers in Neuroinformatics*, *8*(January), 1–13. https://doi.org/10.3389/fninf.2014.00085

Muller, R. U., & Kubie, J. L. (1987). The effects of changes in the environment on the spatial firing of hippocampal complex-spike cells. *The Journal of Neuroscience*, *7*(7), 1951–1968. http://www.ncbi.nlm.nih.gov/pubmed/3612226

Muzzio, I. A., Levita, L., Kulkarni, J., Monaco, J. D., Kentros, C. G., Stead, M., Abbott, L. F., & Kandel, E. R. (2009). Attention enhances the retrieval and stability of visuospatial and olfactory representations in the dorsal hippocampus. *PLoS Biology*, *7*(6). https://doi.org/10.1371/journal.pbio.1000140

Nguyen, P., Abel, T., & Kandel, E. R. (1994). Requirement of a critical period of transcription for induction of a late phase of LTP. *Science*, *265*(5175), 1104–1107. https://doi.org/10.1126/science.8066450

Olypher, A. V, Lánský, P., Muller, R. U., & Fenton, A. A. (2003). Quantifying location-specific information in the discharge of rat hippocampal place cells. *Journal of Neuroscience Methods*, *127*(2), 123–135. https://doi.org/10.1016/S0165-0270(03)00123-7

O'Neill, J., Senior, T., & Csicsvari, J. (2006). Place-selective firing of CA1 pyramidal cells during sharp wave/ripple network patterns in exploratory behavior. *Neuron*, *49*(1), 143–155. https://doi.org/10.1016/j.neuron.2005.10.037

Rashid, A. J., Yan, C., Mercaldo, V., Hsiang, H. L., Park, S., Cole, C. J., Cristofaro, A. De, Yu, J., Ramakrishnan, C., Lee, S. Y., Deisseroth, K., Frankland, P. W., & Josselyn, S. A. (2016). Competition between engrams influences fear memory formation and recall. *Science*, *353*(6297), 383–388. https://doi.org/10.1126/science.aaf0594

Resendez, S. L., Jennings, J. H., Ung, R. L., Namboodiri, V. M. K., Zhou, Z. C., Otis, J. M., Nomura, H., McHenry, J. A., Kosyk, O., & Stuber, G. D. (2016). Visualization of cortical, subcortical and deep brain neural circuit dynamics during naturalistic mammalian behavior with head-mounted microscopes and chronically implanted lenses. *Nature Protocols*, *11*(3), 566–597. https://doi.org/10.1038/nprot.2016.021

Rubin, A., Geva, N., Sheintuch, L., & Ziv, Y. (2015). Hippocampal ensemble dynamics timestamp events in long-term memory. *ELife*, *4*(December), 1–16. https://doi.org/10.7554/eLife.12247

Ryan, T. J., & Frankland, P. W. (2022). Forgetting as a form of adaptive engram cell plasticity. *Nature Reviews Neuroscience*, *23*(3), 173–186. https://doi.org/10.1038/s41583-021-00548-3

Ryan, T. J., Roy, D. S., Pignatelli, M., Arons, A., & Tonegawa, S. (2015). Engram cells retain memory under retrograde amnesia. *Science*, *348*(6238), 1007–1013. https://doi.org/10.1126/science.aaa5542

Scavuzzo, C. J., LeBlancq, M. J., Nargang, F., Lemieux, H., Hamilton, T. J., & Dickson, C. T. (2019). The amnestic agent anisomycin disrupts intrinsic membrane properties of hippocampal neurons via a loss of cellular energetics. *Journal of Neurophysiology*, *122*(3), 1123–1135. https://doi.org/10.1152/jn.00370.2019

Schafe, G. E., Nadel, N. V., Sullivan, G. M., Harris, A., & LeDoux, J. E. (1999). Memory consolidation for contextual and auditory fear conditioning is dependent on protein synthesis, PKA, and MAP kinase. *Learning and Memory*, *6*(2), 97–110. https://doi.org/10.1101/lm.6.2.97

Schuette, P. J., Reis, F. M. C. V., Maechler, P., Chakerian, M., Torossian, A., Blair, G. J., Wang, W., Blair, H. T., Fanselow, M. S., Kao, J. C., & Adhikari, A. (2020). Long-term characterization of hippocampal remapping during contextual fear acquisition and extinction. *The Journal of Neuroscience*, *September*, JN-RM-1022-20. https://doi.org/10.1523/jneurosci.1022-20.2020

Sharma, A. V., Nargang, F. E., & Dickson, C. T. (2012). Neurosilence: Profound Suppression of Neural Activity following Intracerebral Administration of the Protein Synthesis Inhibitor Anisomycin. *The Journal of Neuroscience*, *32*(7), 2377–2387. https://doi.org/10.1523/JNEUROSCI.3543-11.2012

Squire, L. R., & Barondes, S. H. (1974). Anisomycin, like other inhibitors of cerebral protein synthesis, impairs 'long-term' memory of a discrimination task. *Brain Research*, *66*(2), 301–308. https://doi.org/10.1016/0006-8993(74)90148-6

Sweis, B. M., Mau, W., Rabinowitz, S., & Cai, D. J. (2021). Dynamic and heterogeneous neural ensembles contribute to a memory engram. *Current Opinion in Neurobiology*, *67*, 199–206. https://doi.org/10.1016/j.conb.2020.11.017

Vöröslakos, M., Petersen, P. C., Vöröslakos, B., & Buzsáki, G. (2021). Metal microdrive and head cap system for silicon probe recovery in freely moving rodent. *ELife*, *10*(x), 1–21. https://doi.org/10.7554/eLife.65859

Wang, M. E., Wann, E. G., Yuan, R. K., Ramos Álvarez, M. M., Stead, S. M., & Muzzio, I. A. (2012). Long-term stabilization of place cell remapping produced by a fearful experience. *The Journal of Neuroscience*, *32*(45), 15802–15814. https://doi.org/10.1523/JNEUROSCI.0480-12.2012

Wood, E. R., Dudchenko, P. A., & Eichenbaum, H. B. (1999). The global record of memory in hippocampal neuronal activity. *Nature*, *397*(6720), 613–616. https://doi.org/10.1038/17605

Yger, P., Spampinato, G. L. B., Esposito, E., Lefebvre, B., Deny, S., Gardella, C., Stimberg, M., Jetter, F., Zeck, G., Picaud, S., Duebel, J., & Marre, O. (2018). A spike sorting toolbox for up to thousands of electrodes validated with ground truth recordings in vitro and in vivo. *ELife*, *7*, 1–23. https://doi.org/10.7554/eLife.34518

Ziv, Y., Burns, L. D., Cocker, E. D., Hamel, E. O., Ghosh, K. K., Kitch, L. J., El Gamal, A., & Schnitzer, M. J. (2013). Long-term dynamics of CA1 hippocampal place codes. *Nature Neuroscience*, *16*(3), 264–266. https://doi.org/10.1038/nn.3329

519 Methods:

520 **Animals**

521 Sixteen (n = 10 controls, 6 anisomycin) male C57/BL6 mice (Jackson Laboratories), age 16 to
522 22 weeks during behavioral and imaging experiments and weighing 25-32g were used in this
523 study. Three mice were excluded after performing this study: one mouse after histology
524 revealed the GRIN lens implant and viral expression to be medial to the intended imaging, while
525 the other two were excluded due to unstable/overexpression of GCaMP that produced aberrant
526 calcium activity which emerged toward the end of the experiment. After exclusion of these mice,
527 we retained 8 mice in the control (CTRL) group and 5 mice in the anisomycin group (ANI) group.
528 Additionally, behavioral video tracking files for one CTRL mouse were corrupted during
529 recording during all neutral field recordings from day 0 on: this mouse was excluded from all
530 analyses which required using behavior in the neutral arena (e.g., place field correlations and
531 any analyses where the CTRL group was split into Learners and Non-Learners). Mice were
532 socially housed in a vivarium on a 12 hour light-dark cycle with 1-3 other mice prior to surgery
533 and were housed singly thereafter. Mice were given free access to food and water throughout
534 the study. All procedures were performed in compliance with the guidelines of the Boston
535 University Animal Care and Use Committee.

536 One male Long Evans rat, 10 months old and weighing ~480g, was used for the
537 electrophysiological recording in this study. Rats were socially housed in a vivarium on an
538 adjusted 12 hour light-dark cycle (lights on at noon, off at midnight) with 1-3 other rats prior to
539 surgery and given free access to food and water throughout the study. All procedures were
540 performed in compliance with the guidelines of the University of Michigan Animal Care and Use
541 Committee.

542 **Viral Constructs**

543 For mice experiments we used an AAV9.*Syn*.GcaMP6f.WPRE.SV40 virus from the University of
544 Pennsylvania Vector Core/Addgene with an initial titer of ~$4x10^{12}$ GC/mL and diluted it into
545 sterilized potassium phosphate buffered saline (KPBS) to a final titer of ~$2\text{-}4x10^{12}$ GC/mL for
546 injection.

547 For rat experiments, we used an pGP.AAV9.*Syn*.GcaMP7f.WPRE.SV40 virus from the
548 University of Pennsylvania Vector Core/Addgene with an initial titer of $2.6x10^{13}$ GC/mL and
549 diluted it into sterilized phosphate buffered saline (PBS) to a final titer of $2.6x10^{12}$ GC/mL for
550 injection. Due to poor expression no imaging was performed.

551 **Stereotactic Surgery**

552 We performed two stereotactic surgeries and one base-plate implant on naïve mice, aged 3-8
553 months, according to previously published procedures (Kinsky et al., 2018; Resendez et al.,
554 2016). Both surgeries were performed under 1-2% isoflurane mixed with oxygen. Mice were
555 given 0.05mL/kg buprenorphine (Buprenex) for analgesia (subcutaneously, SC), 5.0mL/kg of
556 the anti-inflammatory drug Rimadyl (Pfizer, SC), and 400mL/kg of the antibiotic Cefazolin
557 (Pfizer, SC) immediately after induction. They were carefully monitored to ensure they never
558 dropped below 80% of their pre-operative weight during convalescence and received the same
559 dosage of Buprenex, Cefazolin, and Rimadyl twice daily for three days following surgery. In the
560 first surgery, a small craniotomy was performed at AP -2.0, ML +1.5 (right) and 250nL of

561 GcaMP6f virus (at the titer noted below) was injected 1.5mm below the brain surface at
562 40nL/min using a 1μL Hamilton syringe and infusion pump. The needle remained in place a
563 minimum of 10 minutes after the infusion finished at which point it was slowly removed, the
564 mouse's scalp was sutured, and the mouse was removed from anesthesia and allowed to
565 recover.

566 3-4 weeks after viral infusion, mice underwent second surgery to attach a gradient index (GRIN)
567 lens (GRINtech, 1mm x 4mm). After performing an ~2mm craniotomy around the implant area,
568 we carefully aspirated cortex using blunted 25ga and 27ga needles under constant irrigation
569 with cold, sterile saline until we visually identified the medial-lateral striations of the corpus
570 callosum. We carefully removed these striations using a blunted 31ga needle while leaving the
571 underlying anterior-posterior striations intact, after which we applied gelfoam for 5-10 minutes to
572 stop any bleeding. We then lowered the GRIN lens to 1.1mm below bregma. Note that this
573 entailed pushing down ~50-300μm to counteract brain swelling during surgery. We then applied
574 Kwik-Sil (World Precision Instruments) to provide a seal between skull and GRIN lens and then
575 cemented the GRIN lens in place with Metabond (Parkell), covered it in a layer of Kwik-Cast
576 (World Precision Instruments), and then removed the animal from anesthesia and allowed him
577 to recover after removing any sharp edges remaining from dried Metabond with a dental drill
578 and providing any necessary sutures.

579 Finally, after ~2-4 weeks we performed a procedure in which the mouse was put under
580 light anesthesia to attach a base plate for easy future attachment of a miniature epifluorescence
581 microscope (Ghosh et al., 2011, Inscopix, Inc.). Importantly, no tissue was cut during this
582 procedure. After induction, we attached the base plate to the camera via a set screw, set the
583 camera's focus level at ~1/3 from the bottom of its range, and carefully lowered the camera
584 objective and aligned it to the GRIN lens by eye, and visualized fluorescence via nVistaHD until
585 we observed clear vasculature and putative cell bodies expressing GcaMP6f (Resendez et al.,
586 2016). To counteract downward shrinking during curing, we then raised the camera up ~50μm
587 before applying Flow-It ALC Flowable Composite (Pentron) between the underside of the
588 baseplate and the cured Metabond on the mouse's skull. After light curing, we applied opaque
589 Metabond over the Flow-It ALC epoxy to the sides of the baseplate to provide additional
590 strength and to block ambient light infiltration. Mice were allowed to recover for several days
591 prior to habituation to camera attachment and performance of the behavioral task outlined
592 below. In the event that we did not observe clear vasculature and cell bodies when we first
593 visualized fluorescence we covered the GRIN lens with Kwik-Cast and removed the mouse from
594 anesthesia without attaching the baseplate. We then waited an additional week and repeated
595 the steps above.

596 For rats, we performed two surgeries in a similar manner as described above for mice.
597 However, rats were administered pre-operative and post-operative Meloxicam orally for
598 analgesia (in lieu of Buprenex) and triple-antibiotic was applied locally (in lieu of Cefazolin
599 injections) to the incision at the end of surgery. Meloxicam was additionally administered for two
600 days post-surgery during recovery, and animals were monitored daily for a minimum of seven
601 days during recovery. 0.4mL of a lidocaine/bupivacaine cocktail were given under the scalp to
602 provide local anesthesia at the incision site. In the first surgery, 1000nL of GcaMP7f virus was
603 infused in the prelimbic cortex at the center of a 1mm craniotomy (AP + 2.9, ML + 3.6, from
604 Bregma, DV -3.0 at an 18 degree angle from top of brain). Following infusion, ~1.5 mm of
605 overlying cortex was removed and a 23ga needle was lowered to ~500μm above the target site.

606 Then, a 0.6 x 7 mm GRIN lens was lowered to 3.0mm below the top of the brain, the area
607 between the skull and lens was sealed with Kwik-Sil, and the lens was affixed to the skull with
608 Vivid-Flow light-curable composite (Pearson Dental) and Metabond (Parkell). The lens was then
609 covered in Kwik-Sil for protection. During this surgery, ground and reference screws were also
610 placed over the cerebellum and a 3d printed crown base was attached to the rat's skull
611 (Vöröslakos et al., 2021) to which crown walls and top were connected and to further protect the
612 lens and future microdrive/probe implant. The rat was screened for fluorescence 8-12 weeks
613 later, but no cell dynamics were observed so no imaging equipment was implanted for this rat.

614 16 weeks later, the rat was again given pre-operative Meloxicam and anesthetized under
615 isoflurane. The crown walls were removed and a 1.0mm craniotomy was performed at AP-4.8,
616 ML+3.6 from bregma. After removing dura and stopping bleeding with cold, sterile saline, a
617 NeuroNexus A1x32-5mm-50-177 probe, attached to a metal microdrive, was implanted at 2.3
618 mm below the brain surface and the metal drive base was attached to the skull with Unifast light
619 cured dental epoxy (Henry-Schein). The craniotomy was sealed with Dow-Sil, the probe was
620 protected with dental wax, and the ground and reference wires were connected to the probe
621 electronic interface board (EIB). The crown walls were re-attached, the EIB was connected to
622 the crown walls, and the rat was removed from isoflurane and allowed to recovery. The rat was
623 monitored daily for 7 days prior to recording, during which the probe was lowered ~1mm until
624 sharp wave ripples and spiking activity were visualized indicating localization of the probe in the
625 CA1 cell layer.

626 **Histology procedures**

627 Hippocampal slices were prepared following extraction from mice in accordance with the
628 standard methods and guidelines of the Boston University Animal Care and Use Committee. In
629 brief, mice were euthanized with Euthasol (Virbac), transcardially perfused with
630 paraformaldehyde (PFA), and decapitated. Following extraction, brains were placed in PFA for
631 approximately 48 hours before undergoing sectioning. Brains that were sliced using a Cryostat
632 underwent an additional step of sucrose cryoprotection and subsequent freezing in -80C. Brains
633 were mounted to the slicing platform using Tissue Tek O. C. T. (Sakura) and kept at -30C
634 throughout sectioning. 50µm slices were collected across the entire aspiration site in the dorsal
635 hippocampus region. Brains that were sliced using a vibratome were stabilized using super glue
636 and submerged in 1% PBS. A Leica VT1000 S vibratome was equipped with a platinum coated
637 double edged blade (Electron Microscopy Sciences , Cat. #72003-01) and set to a maximal
638 speed of 0.9mm/s for collecting 50 µm slices. Slices prepared from both the cryostat and
639 microtome were directly mounted onto (type of slides go here) and cover-slipped using DAPI
640 following sectioning. No histology was performed in the rat study.

641 **Behavioral Paradigm**

642 Prior to surgery mice were handled to habituate them subsequent camera attachment. 3-7 days
643 following base plate attachment surgery we conditioned mice to the imaging procedures by
644 further handling them for 5-10 minutes for a minimum three days. During this handling a plastic
645 "dummy" microscope (Inscopix) of approximately the same size/weight as the imaging camera
646 was attached to each mouse's head and remained on his head for 1-2 hours in his home cage.
647 When it became easy to attach the scope to the mouse's head a real imaging miniscope was
648 attached to head and an optimal focus plane chosen. We then recorded three 5 minute imaging
649 videos at this focus and +/- ¼ turn (~25µm) in the mouse's home cage. These movies were

processed as described in the Image Acquisition and Processing section and an optimal zoom was chosen based on whichever focus plane maximized cell yield and produced clear looking cell bodies. Animals were then placed in a novel environment with a different size and shape compared to the experimental environments for a 10 minute session to habituation them to the general experimental outline and ensure that they explored novel arenas.

Following habituation to the imaging procedures mice performed a contextual fear conditioning (CFC) task with simultaneous imaging of hippocampus neurons over the course of 10 days. Note that all recording sessions are referred to by their time relative to applying the mild foot-shock and the arena in which the recording occurred: e.g., Shock Day -2 occurred in the shock arena two days prior to foot-shock while Neutral 4 hours occurred four hours after foot-shock in the neutral arena. A typical day (Days -2, -1, 1, 2, and 7) consisted of two separate 10 minute recording blocks/sessions: one in the Neural arena and one in the shock arena. Mice first explored a square (neutral) arena, placed in the center of a well-lit room, for 10 minutes. The neutral arena was a square constructed of 3/8” plywood (25cm x 25cm x 15 cm), which was painted yellow with sealable paint. Additionally, one wall was painted with black horizontal stripes for visual orientation purposes. The neutral arena was wiped down with 70% ethanol ~10 minutes prior to recording. After 10 minutes of exploration the experimenter took the mouse out of the arena, leaving the miniscope camera on their head and placed the mouse in its home cage on a moveable cart upon which it was immediately transported down a short hallway to second room.

The second room was dimly lit and contained the fear conditioning (shock) arena. The shock arena (Coulbourn Instruments, Whitehall, PA, USA) consisted of metal-panel side walls, Plexiglas front and rear walls, and a stainless-steel grid floor composed of 16 grid bars (22cm x 22cm). Following 10 minutes of exploration of the shock arena, mice were removed from the arena, the camera was removed, and mice were returned to their home cage. Both arenas were wiped down with 70% ethanol ~10min prior to recording to eliminate any odor cues. Note that mice always explored the neutral arena first and the shock arena second. For the Day 0 sessions, mice first explored the neutral arena for 10 minutes and were transported to the shock arena as usual. However, during this session (Shock Day 0) the mouse was immediately given a single 0.25mA shock and allowed to explore the arena for an additional 60 seconds only before being removed and returned to his cage. Efficacy of shock was confirmed post-hoc by eye by the presence of jumping/darting behavior immediately post-shock. The 4 hour session was identical to the Day -2, 1, 1, 2, and 7 sessions. With the exception of the 4 hour session, all recording sessions were performed in the first half of the mouse’s life cycle while the 4 hour session occurred in the second half of the light cycle.

On day zero, after the camera was removed and prior to returning to their home cage, mice received an intraperitoneal injection of either anisomycin (150 mg/kg, Sigma-Aldrich A9789) or the equivalent amount of vehicle. After injection, they were returned to their cage for 4 hours until the next recording session began.

Following extensive habituation to a rest box during the seven day recovery period, rat neural activity and behavior was recorded across ~ 5 hours. Following a 15 minute baseline recording (PRE) in the rest box, the animal was given an I.P. injection of anisomycin and then immediately placed on a novel linear track which he explored for 45 minutes (TRACK). The rat was then placed back into the rest box for 3.5 hours (POST). Following that, the animal was placed on a second novel track for 45 minutes (TRACK) followed by a brief recording in the rest box

(POST2). Data was acquired continuously throughout with the exceptions of periodic cable disconnections to perform the I.P. injection, start a new recording epoch, and disconnect/reconnect cables that became twisted.

Anisomycin

For mice recordings, 25 mg of anisomycin was dissolved into 50 µL of 6N HCl and 500 µL of 1.8%NaCl. ~125 µL of 1N NaOH was then added to the solution followed by 0.1-0.5 µL of 1N NaOH, testing pH after each addition until a final pH of 7.0 to 7.5 was reached, with a final concentration of 24-27 mg/mL. In the case that pH rose above 7.5 during titration and and/or the anisomycin went back into precipitate, small amounts (10-20 µL) of 6N HCl were added until particles were no longer visible and the titration with 1N NaOH was restarted. Mice were administered 150mg/kg of anisomycin solution via intraperitoneal injection, or ~0.15-0.18mL for a typical 30g mouse.

For rat recordings, 100mg of anisomycin was dissolved into 1.6mL of 0.1N HCl (in 0.9% saline). ~240 µL of 1N HCl was added, then 10-12 µL of NaOH was added in 1-2 µL amounts, testing pH between each step until a pH of 7-7.5 was reached. 0.9% Saline was then added until a final concentration of 33 mg/mL was reached. Due to a small amount of waste, the final amount injected was 50mg (1.5 mL) which corresponds to 100 mg/kg for the rat.

Behavioral Tracking and Fear Metrics

We utilized two different camera/software configurations for tracking animal behavior. Both configurations generated a TTL pulse at the beginning of behavioral tracking to synchronize with image acquisition. We utilized Cineplex software (v2, Plexon) to track animal location at 30Hz in the neutral arena. We used FreezeFrame (Actimetrics) to track animal location in the shock arena at 3.75Hz. Animal location was obtained post-hoc via custom-written, freely available Python software (www.github.com/wmau/FearReinstatement). We observed inconsistent frame rates and inaccurate acquisition of behavioral video frames for one mouse in the neutral arena during the day 0, 4 hour, and day 1-2 sessions. These sessions were excluded from analysis.

Freezing was calculated by first dowsampling neutral position data to 3.75 Hz to match the sample rate used in the shock arena. We then identified freezing epochs as any periods of 10 consecutive frames (2.67 seconds) or more where the mouse's velocity was less than 1.5cm/second.

Neural Discrimination

We evaluated the extent to which each animal's behavior reflected the expression of a context-specific fear memory through a behavioral discrimination index (DI_{beh}), calculated as follows:

$$DI_{beh} = \frac{Frz_{Neutral} - Frz_{Shock}}{Frz_{Neutral} + Frz_{Shock}}$$

Where $Frz_{Neutral}$ and Frz_{Shock} are the percentages of time spent freezing in the neutral and shock arenas, respectively. Thus, a negative DI_{beh} value indicated more freezing behavior in the shock arena (indicating successful encoding of a context-specific fear memory), a positive DI_{beh} value indicated more freezing behavior in the neutral arena, and a DI_{beh} value around zero indicated equal/low freezing behavior in each arena (indicating the formation of a non-specific or weak fear memory).

Imaging Acquisition and Processing

Brain imaging data was obtained using nVista HD (Inscopix) at 720 x 540 pixels and a 20 Hz sample rate. Note that imaging data for one mouse was obtained at 10 Hz. Prior to neuron/calcium event identification we first pre-processed each movie using Inscopix Imaging Suite (Inscopix) software. Preprocessing entailed three steps a) motion corrections, and b) cropping the motion-corrected movie to eliminate any dead pixels or areas with no calcium activity, and c) extracting a minimum projection of the pre-processed movie for later neuron registration. We did not analyze one imaging session in which we had to reconnect the camera cable mid-session and could not synchronize the imaging data with behavioral data. Maximum projections of imaging movies were made using the Inscopix Imaging Suite or custom-written functions based off of an open-source MATLAB library (Muir & Kampa, 2015).

Electrophysiological Recordings

Data was acquired using an Intan 1028 channel recording system through OpenEphys software into binary format and behavior was tracked via Omnitrack high resolution cameras.

Data Analysis

Data analysis was performed in both Python and MATLAB software. Python analysis code is available at https://github.com/nkinsky/Eraser.

Spike sorting and analysis

Electrophysiological recordings were automatically clustered using SpyKING CIRCUS software (Yger et al., 2018) and units were manually curated in phy. Units were grouped into single units if they exhibited a clear refractory period and were well-isolated from other putative spikes. Other units which exhibited a clear waveform but were either poorly isolated or exhibited refractory period violations were classified as multi-unit activity (MUA). All single units and MUA were combined and cross-correlograms for the combined activity were created for each epoch of the recording separately.

Tenaspis

Neuron regions-of-interest (ROIs) and calcium events were identified using a custom written, open source algorithm employed in MATLAB 2016b called A Technique for Extracting Neuronal Activity from Single Photon Neuronal Image Sequences (Tenaspis) (Mau et al., 2018). This procedure was comprehensively documented in Kinsky et al., 2018:

"Tenaspis is open-source and available at: https://github.com/SharpWave/TENASPIS. First, Tenaspis filters each calcium imaging movie with a band-pass filter per (Kitamura et al., 2015) to accentuate the separation between overlapping calcium events. Specifically, Tenaspis smooths the movie with a 4.5 μm disk filter and divides it by another movie smoothed with a 23.6 μm disk filter. Second, it adaptively thresholds each imaging frame to identify separable pockets of calcium activity, designated as blobs, on each frame. Blobs of activity are accepted at this stage of processing only if they approximate the size and shape of a mouse hippocampal neuron, as measured by their radius (min = ~6μm, max = ~11μm), the ratio of long to short axes (max = 2), and solidity (min = 0.95), a metric used by the *regionprops* function of MATLAB we employ to exclude jagged/strange shaped blobs. Third, Tenaspis strings together blobs on successive frames to identify potential calcium transients and their spatial activity patterns.

Fourth, Tenaspis searches for any transients that could results from staggered activity of two neighboring neurons. It rejects any transients whose centroid travels more than 2.5μm between frames and whose duration is less than 0.20 seconds. Fifth, Tenaspis identifies the probable spatial origin of each transient by constructing putative regions-of-interest (ROIs), defined as all connected pixels that are active on at least 50% of the frames in the transient. Sixth, Tenaspis creates initial neuron ROIs by merging putative transient ROIs that are discontinuous in time but occur in the same location. Specifically, it first attempts to merge all ROIs whose centroids are less than a distance threshold of ~0.6μm from each other. In order to merge two transient ROIs, the two-dimensional Spearman correlation between the ROIs must yield $r^2 > 0.2$ and $p < 0.01$. Tenaspis then successively increases the distance threshold and again attempts to merge ROIs until no more valid merges occur (at a distance threshold of ~3μm, typically). Seventh, Tenaspis integrates the fluorescence value of each neuron ROI identified in the previous step across all frames to get that neuron's calcium trace, and then identifies putative spiking epochs for each neuron. Specifically, it first identifies the rising epochs of any transients identified in earlier steps. Then, it attempts to identify any missed transients as regions of the calcium trace that have a) a minimum peak amplitude > 1/3 of the transients identified in step 3, b) a high correlation ($p < 0.00001$) between active pixels and the pixels of the average neuron ROI identified in step 6, and b) a positive slope lasting at least 0.2 seconds. Last, Tenaspis searches for any neuron ROIs that overlap more than 50% and whose calcium traces are similar and merges their traces and ROIs."

Between Session Neuron Registration

We utilized custom-written, freely available MATLAB code (available at https://github.com/nkinsky/ImageCamp) to perform neuron registration across sessions in accordance with previous results (Kinsky et al., 2018). The details of this procedure described in Kinsky et al. (2018) are reproduced here:

"Neuron registration occurred in two steps: session registration and neuron registration.

Session registration – Prior to mapping neurons between sessions, we determined how much the imaging window shifted between sessions. In order to isolate consistent features of the imaging plane for each mouse (such as vasculature or coagulated blood), we created a minimum projection of all of the frames of the motion-corrected and cropped brain imaging movie for each recording session. One session ("registered session") was then registered to a base session using the "imregtform" function from the MATLAB Image Processing Toolbox, assuming a rigid geometric transform (rotation and translation only) between images, and the calculated transformation object was saved for future use.

Neuron Registration – Next, each ROI in the registered session was transformed to its corresponding location in the base session. Each neuron in the base session was then mapped to the neuron with the closest center-of-mass in the registered session, unless the closest neuron exceeded our maximum distance threshold of 3 pixels (3.3 μm). In this case the base session neuron was designated to map to no other neurons in the registered session. If, due to high density of neurons in a given area, we found that multiple neurons from the base session mapped to the same neuron in the registered session, we then calculated the spatial correlation (Spearman) between each pair of ROIs and designated the base session ROI with the highest correlation as mapping to the registered session ROI.

For multiple session registrations, the same procedure as above was performed for each session in two different ways. First, we registered each session directly to the first session in the experiment and updated ROI locations/added new ROIs to set of existing ROIs with each registration. This helped account for slight day-to-day drift in neurons ROIs due to shifts in vasculature, build-up of fluid underneath the viewing window, creep/shrinkage of dental cement, etc. Second, to ensure that neuron ROIs did not drift excessively across sessions we also performed all the above steps but did NOT update ROI locations allowing us to register each set of ROIs to those furthest away chronologically. The resulting mappings were then compared across all sessions, and any neuron mappings that differed between the two methods (e.g., ROIs that moved excessively across the duration of the experiment) were excluded from analysis. Those that remained in the same location were included."

The procedure to assess the quality of across session registration was described in Kinsky et al. (2018) and is reproduced here: "We checked the quality of neuron registration between each session-pair in two ways: 1) by plotting the distribution of changes in ROI orientations between session and comparing it to chance, calculated by shuffling neuron identity between session 1000 times, and 2) plotting ROIs of all neurons between two sessions and looking for systematic shifts in neuron ROIs that could lead to false negatives/positives in the registration." All session-pairs (except those few in which we could not synchronized imaging and behavioral data as noted above) met the above two criteria and were thus included in our analysis.

Cells that had calcium activity in the first session (neutral arena) for which we did not identify a matching neuron in the second session (shock arena) were classified as OFF cells. Likewise, neurons active in the shock arena with no matching partner in the neutral arena were classified as ON cells.

All neuron registrations were cross validated by overlaying ROIs from each session and evaluating their match by eye. In a few cases, we noticed erroneous registrations and adjusted our between-session neuron alignment by calculating the rigid geometric transformation using 4-5 cell ROIs active in both sessions.

Neural Discrimination Metrics

The extent to which gross hippocampal ensemble activity differed between arenas was calculated in two ways. First, we calculated the proportion of cells that turned ON and OFF between arenas divided by the total number of cells active in either arena.

Next, we calculated the extent to which each neuron active in both arenas distinguished between arenas by changing its event rate in a manner analogous to $DI_{Fr.}$ However, we took the absolute value to account for the fact that both positive and negative event rate changes could reflect neural differentiation between arenas. Then, we took the mean across all neurons to obtain a neural discrimination index (DI_{Neuron}):

$$DI_{Neuron} = \left| \frac{ER_{Neutral} - ER_{Shock}}{ERz_{Neutral} + ER_{Shock}} \right|$$

Placefield Analysis

Calcium transients occurring when the mouse was running greater than or equal to 1.5cm/second were spatially binned (1cm by 1cm) and occupancy normalized following which place fields were identified and quantified in a manner similar to Kinsky et al. (2018), reproduced here:

"Spatial mutual information (SI) was computed from the following equations, adapted from (Olypher et al., 2003)

$$I_{pos}(x_i) = \sum_{k=0}^{1} P_{k|x_i}\, log\left(\frac{P_{k|x_i}}{P_k}\right)$$

$$SI = \sum_{i=1} P_{x_i}\, I_{pos}(x_i)$$

where:

- P_{xi} is the probability the mouse is in pixel x_i
- P_k is the probability of observing *k* calcium events (0 or 1)
- $P_{k|xi}$ is the conditional probability of observing *k* calcium events in pixel x_i.

The SI was then calculated 1000 times using shuffled calcium event timestamps, and a neuron was classified as a place cell if it 1) had at least 5 calcium transients during the session, and 2) the neuron's SI exceeded 95% of the shuffled Sis…We defined the extent of a place field as all connected occupancy bins whose smoothed event rate exceeded 50% of the peak event rate occupancy bin."

Since spatial mutual information is biased by the number of samples (Olypher et al., 2003), we re-sampled the behavioral tracking data to match that of the imaging data (20Hz). This required up-sampling the shock arena data (3.75Hz->20Hz) and down sampling the neutral arena data (30Hz->20Hz).

Placefield similarity between sessions was assessed by first smoothing the 2-d occupancy normalized event rate maps with a gaussian kernel (2.5cm std), flattening the smoothed maps into a vector, and then performing a Spearman correlation between all neurons active in both sessions. To quantify chance-level place field similarity we randomly shuffled the mapping between neurons from the first to the second session before performing the Spearman correlation. We then repeated this procedure 100 times.

To assess the possibility that the configuration of place fields rotated together coherently between sessions (Kinsky et al., 2018), we again performed a Spearman correlation but after rotating the 2-d occupancy map in the second session 90 degrees. Since, due to small camera distortions, some 2-d occupancy maps were not square, one some occasions we resized (minimally) the second map to match the size/shape of the first map using the reshape function in Python's numpy package prior to correlate the two maps. We repeated this in successive 90 degree increments and then took the mean correlation of all neurons that were active in both sessions to determine the optimal/"best" rotation of the place field map as that which maximized the correlation between sessions.

We also performed a “center-out” rotation analysis to assess coherent place field rotations between sessions. First, the angle to the pixel with the maximum occupancy normalized event rate was identified for each cell. Second, this angle was recalculated for the same cell in a different session in the same box. These two angles were subtracted to get the “center-out” rotation between sessions. Sessions which exhibited a coherent rotation displayed a peak in a histogram of center-out angles at 0, 90, 180, or 270 degrees, while sessions which exhibited global remapping exhibited a uniform distribution of rotation angles.

Freeze-predicting Cell Analysis

Freeze onset and offset times were first identified for each mouse/session as noted in the *Behavioral Tracking and Fear Metrics* section above. We then formed calcium event rasters using the neural activity for each cell +/- 4 seconds from freeze onset, organizing the data into a *nfreeze_onsets x ntime_bins* array. We then summed this raster along the 0th dimension to get a freeze tuning curve. To calculated significance, we randomly, circularly shifted the putative spiking activity for a cell and calculated a shuffled tuning curve in a similar manner to the actual data. We repeated this procedure 1000 times, and calculated significance for each time bin as the number of shuffles where the shuffled tuning exceeded the actual tuning curve divided by 1000. Last, we designated cells as significantly freeze-tuned if they had 3 or more bins with $p < 0.01$ and were active on at least 25% of freezing events.

Covariance Analysis

Putative spiking activity for each cell was first binned into 0.5 second windows and z-scored after binning, forming a *ncells x nbins* array. The covariance of this array was then calculated using the *cov* function in numpy, returning a *ncells x ncells* array. For between-session comparisons, cells active in both sessions were registered and a new array was formed with the base (1st) session covariance in the lower diagonal and the registered (2nd) session in the upper diagonal. All entries along the main diagonal were ignored. This analysis was also performed including only peri-freeze times (to assess peri-freeze covariance), after randomly downsampling the number of freeze epochs to match the average from days -2 and -1 (to control for increased sampling on days 1 and 2), and after excluding all peri-freeze times (to assess non peri-freeze covariance).

Coactivation Analysis

Putative spiking activity was first binned relative to the start of each freezing epoch (“freeze onset”), yielding a *nfreeze_onsets x nbins* array of binarized neural activity (1 = active, 0 = inactive). Pairwise coactivation was then calculated by taking the dot product of the binarized neural activity arrays between each pair of cells and taking the mean along the first axis, yielding the probability that both cells in a given cell-pair were active in each sampling bin. To calculate population-level coactivity, the number of active cells was first calculated for each recording session. The average number of active cells was then calculated across all peri-freeze trials (+/- 4 seconds) and this number was z-scored relative to activity across the entire session. To determine which cell-pairs exhibited significant pairwise coactivity beyond chance level, we first formed a *nfreeze_onsets x nbins* array of neural activity for each cell in a pair. We then randomly permuted the rows of the array for the second cell in the pair and calculated a shuffled level coactivation probability for that pair as described above. We repeated this process 100 times for each cell pair, and then calculated a p-value for each bin as 1 – (# of bins where

shuffle exceeds actual coactivity) / 100. A cell-pair was designated to have significant pairwise coactivation if it had > 3 consecutive bins with $p < 0.05$.

FIGURE LEGENDS

Figure 1: Neural discrimination between arenas predicts specificity of fear learning. A) Schematic of the behavioral paradigm. Mice freely explored two distinct arenas (neutral and shock) for 10 minutes each day. Mice underwent mild contextual fear conditioning on day 0 in the shock arena followed by immediate I.P. administration of anisomycin or vehicle in their home cage. Memory recall tests were conducted 4 hours and 1, 2, and 7 days post-shock. The time of each session is referenced to the shock session. **B)** (left) Learner (CTRL) mice freezing on all days. Red = shock arena, blue = neutral arena. *p=1.3e-0.5 shock – neutral freezing from days -2/-1 to days ½ one-sided t-test (n=4 mice). (right) Same but for Non-Learner (CTRL) mice (n=3 mice). **C)** (left) Neural overlap plots between neutral and shock arenas for an example Learner mouse on day -1, before shock. Green = cells active in the shock arena only, yellow = cells active in the neutral arena only, orange = cells active in both arenas. (right) Same for example Non-Learner on day -2 showing higher overlap of active cells between arenas. **D)** Same as B but for ANI group **E)** Mean neural discrimination between arenas (same day, days -2 to -1 and 1 to 2) vs. within arenas (same arena, days -2 and -1, days 1 and 2). *p=2.35e-8 (ρ=-0.56) Spearman correlation**. F)** Example calcium activity from the Learner mouse shown in C (left) for cells active in both arenas. Black = calcium trace, red = putative spiking activity during transient rises. Top row shows shock arena preferring cells, bottom row shows neutral arena preferring cells. **G)** Behavioral discrimination between arenas after shock (Days 1-2) shows formation of a specific fear memory for Learners only, by definition (positive = more freezing in neutral arena, negative = more freezing in shock arena, 0 = equal freezing in both arenas). *p=0.022, **p=0.00038 1-sided t-test **H)** Neural discrimination between arenas BEFORE shock indicates Learners formed more distinct representations of each arena prior to learning. Same conventions as F. *p=0.030, +p=0.059 two-sided t-test. **I)** Neural overlap between arenas correlates with specificity of fear memory on days 1-2 for Learners but not Non-Learners. *p=0.033 (ρ=0.61). **J)** Same as I) but plotting neural overlap vs. behavioral discrimination between arenas. +p=0.059 (ρ=-0.56) for Learners.

Figure 2: Anisomycin accelerates cell turnover and stifles learning-related place field remapping A) Cell overlap ratio with Day -2 session, CTRL group. Blue = within shock arena, red = shock v. neutral arena. **B)** Same as A) but for ANI group. **C)** Change in overlap ratios from a and b. *p=0.028, **p=0.00024 two-sided t-test. **D)** Number of active neurons observed each day, normalized to day -1. *p=0.039 two-sided t-test. **E)** Stable place field. (*top)* Example mouse trajectory (black) with calcium activity (red) overlaid for the same cell from day -2 to -1 in shock arena, *(bottom)* occupancy normalized rate maps for the same cells. **F)** Remapping place field. Same as E) but for a different cell that remaps from day -2 to day 1 in the shock arena. **G)** Place field correlations for all mice before shock (Days -2 and -1). *p<0.0032 Learners vs ANI and Non-Learners vs ANI, **p=1.9e-6 Non-Learners vs ANI, k-s test after Bonferroni correction. Inset shows mean +/- 95% CI. **H)** Same as G) but for days after shock. *p=0.045 Learners vs Non-Learners and p=0.0059 Non-Learners vs ANI, +p=0.1 Learners vs ANI. **I)** Same as G) but to assess learning-related remapping from before to after shock. *p=0.00021 Learners vs Non-Learners and p=3.4e-11 Non-Learners vs ANI, +p=0.12 Learners vs ANI. **J)** Place field correlations before shock broken down by mouse. **K)** Same as J) but for sessions after shock. **L)** Same as J) but from before to after shock. p=0.002 mixed ANOVA, group x arena interaction. *p=0.025 Non-Learners vs ANI, **p=0.013 Learners vs Non-Learners, ***p=0.034 Learners vs ANI, post-hoc pairwise t-test after Bonferroni correction. Boxplots denote median and 1st/3rd quartiles, whiskers = 1.5 x interquartile range, gray solid/dashed line indicates mean +/- 95% CI for shuffled distribution.

Figure 3: ANI administration suppresses the development of coordinated freeze-predicting neural activity. **A) and B)** Example traces from two freeze-predicting cells which exhibit coordinated activity prior to freezing event during the day 1 memory recall session in the shock arena. Red = putative spiking activity, pink = cell shown in C, blue = cell shown in E. **C)** After learning (Days 1 and 2), z-scored population level calcium activity peaks between 0 and 2 seconds prior to freezing for CTRL relative to the ANI group. Line/shading = mean +/- 95% CI. Red: bins with $p < 0.05$, independent t-test (two-sided). **D) and E)** Example Learner freeze-predicting cells identified during the 4 hour (D) or day 1 (E) memory test tracked across sessions. Peri-event calcium activity rasters are centered on freeze onset time (solid green). Dashed green = baseline calcium event probability, red solid = peri-freeze calcium event probability, bins with p<0.01 (circular permutation test) noted with red bars at top. D/E corresponds to

pink/blue cells shown in A-B. Bold = session with significant freeze-tuning. **F)** Same as D and E but for ANI mouse immobility-predicting cell identified during the 4 hour session. **G)** Peri-freeze calcium event probability for all freeze-predicting cells detected for each group after learning (Days 1-2), sorted by time of peak activation. **H)** (left) Cumulative distribution of peak peri-freeze activation times before learning. *p=0.49, **p=1e-5 two-sided Wilcoxon rank-sum test , c: p=0.005 Non-Learners v. ANI, 1-sided Mann-Whitney U-test. (right) same as left but for after learning. *p < 0.022, **p=2e-7 two-sided Wilcoxon rank-sum test. a: p=0.022 Learners v. Non-Learners, b: p=0.029 Learners v. ANI 1-sided Mann-Whitney U-test. **I)** Proportion of freeze-predicting cells detected each day across all groups. Green = freezing epochs. **J)** Change in peak peri-freeze calcium event probability for all freeze-predicting cells detected during the 1 day session. p < 0.02 1-way ANOVA each day separately, *p=0.02, **p=0.001, ***p=0.0006 post-hoc Mann-Whiney U-test. **K)** Freeze-predicting cells exhibit increased peri-freeze covariance for Learners but not Non-Learners or ANI group mice. Mean covariance of freeze-predictive cells from each session shown. p=0.047 two-way ANOVA. *p=0.001 post-hoc pairwise t-test (two-sided) after Bonferroni correction. **L-N)** Pairwise coactivation probability of all freeze-predicting cells during Before, 4 hour, and After sessions. Maroon/Black bars at top indicate significant increases in coactivation at 4 hour / After time points compared to before, p< 0.01 1-sided Mann-Whitney U-test. **O)** Proportion of freeze/immobility-predictive cells with significant pairwise coactivation compared to chance (trial shuffle). Line/shading = mean +/- 95% CI. p=0.02 two-way ANOVA. *p=0.036, **p=0.0014 post-hoc pairwise Mann-Whitney U-test after Bonferroni correction.

Figure S1: **CTRL animals exhibit behavioral variability following learning and similar rates of cell turnover between arenas vs. across days.**

A) CTRL mice freezing on all days. Red = shock arena, blue = neutral arena *p=0.025 shock - neutral freezing from days -2/-1 to days 1/2, one-sided t-test (n=7 mice). **B)** Distribution of DI_{beh} scores for all mice in CTRL group on days 1 and 2. Dashed line indicates cutoff between Learners and Non-Learners. **C)** Cell overlap 1 day apart in the same arena (days -2 to -1 and 1 to 2) vs. cell overlap between arenas on the same day (days -2, -1, 1, 2) for all mice in CTRL group. *p=1.7e-5, r=0.74 Spearman correlation.

Figure S2: Non-specific effects of Anisomycin include a reduction in locomotion

A) 4 mice were given I.P injections of anisomycin only (no shock) and their locomotion was tracked over 24 hours. Normal activity did not return to baseline until between 6 and 24 hours later.

Figure S3: **Coherent Place Field Rotations Observed Between Sessions**

A) Example animal trajectories from neutral arena day -2 (top row) and day -1 (middle row) with calcium activity overlaid (red). Each column corresponds to one cell. Bottom row shows data rotated 90 degrees, demonstrating a coherent rotation of spatial activity for all neurons. **B)** Smoothed, occupancy normalized calcium event maps corresponding to data shown in A). **C)** The angle from the center of the arena to each cell's maximum intensity place field center was calculated for each session (center-out angle). The distribution of center-out angles plotted, demonstrating a coherent rotation of place fields from Day -2 to Day -1 by 90 degrees. **D)** Place field correlations (smoothed event maps) between sessions indicate apparently low stability across days without considering rotations, giving the false impression that the place field map randomly reorganizes between sessions. **E)** High correlations were observed after considering a coherent 90 degree rotation between sessions, indicating that place fields retain the same relative structure but rotate together as a whole. **F)** Mean correlations for each mouse and **G)** combined correlations for all neurons calculated without considering rotations gives the impression of instability before/after shock and heightened remapping for all groups from before to after learning.

Figure S4: Place field correlations with STM (4 hour) session

A) Distribution of place field correlations for all mice combined for sessions before (Day -2 and Day -1) vs 4 hour session. **B)** Same as A) but for 4 hour vs days 1-2 sessions. *p=0.0217 Non-Learners v ANI in shock arena, **p=0.00014 Non-Learners v ANI neutral arena, ***p=3.6e-8 Learners v Non-Learners neutral Arena. All p-values after Bonferroni correction for 3 comparisons. **C)** Before v STM mean place field correlations for each mouse/session-pair. **D)** Same as C but for STM v After.

Figure S5: Population Vector (PV) correlations indicate that anisomycin disrupts cell turnover

A)-E) 1D PV correlations between sessions including only cells active in BOTH sessions. **A)** Before (Days -2 and -1), *p=0.006 shock v neutral arena, mixed ANOVA. **B)** After (Days 1 and 2) *p=0.024 shock v neutral arena, mixed ANOVA. **C)** Before v After, p < 0.003 neutral v shock arena and Group x Arena interaction, mixed ANOVA. *p<0.001, +p=0.056 t-test (two-sided) after Bonferroni correction. **D)** Before v STM (4 hour), p=0.052 Group x Arena interaction, mixed ANOVA. **E)** STM v After *p=0.004 Neutral v Shock arena, mixed ANOVA. **F)-J)** 1D PV correlations including cells active in EITHER session (includes new and silent cells). **F)** Before *p<0.001 shock v neutral arena, mixed ANOVA. **G)** After, p > 0.12 all comparisons mixed ANOVA. **H)** Before v After, p<0.003 all comparisons mixed ANOVA *p=0.023 Learners v ANI, **p=0.007 Non-Learners v ANI, +p=0.083 Non-Learners v ANI t-test (two-sided) after Bonferroni correction. **I)** Before v STM p<0.005 Arena and Group comparisons, p=0.059 Arena x Group interaction, *p=0.004 Learners v ANI, **p=0.033 Learners v ANI t-test (two-sided) after Bonferroni correction. **J)** STM v After p<0.022 Arena and Group comparisons, p=0.103 Arena x Group interaction, *p=0.041 Learners v ANI, **p=0.003 Non-Learners v ANI, ***p=0.003 Non-Learners v ANI t-test (two-sided) after Bonferroni correction**.** Green = Learners, Orange = Non-Learners, Blue = ANI.

Figure S6: Freeze-cell covariance increases are driven by Learners and not purely a result of less freezing in Non-Learners and the ANI group.

A)-C) Example freeze-predicting/immobility cells tracked across sessions forward and backward in time from the day indicated in bold. Peri-event calcium activity rasters are centered on freeze onset time (solid green). Dashed green = baseline calcium event probability, red solid = peri-freeze calcium event probability, bins with p<0.01 (circular permutation test) noted with red bars at top. D/E corresponds to pink/blue cells shown in A-B. **A)** Example immobility cell from Non-Learner **B)-C)** Example freeze-predicting cells from two different Learners. **D)** Proportion freeze/immobility predicting cells detected in neutral arena across days. **E)** Mean covariance of all cells in neutral arena prior to learning exhibit small changes, compare y-axis to Figure 3K and S6G. p=0.012 two-way ANOVA, *p=0.002 post-hoc pairwise two-sided Mann-Whitney U-test after Bonferroni correction. **F)** Mean covariance of freeze/immobility-predicting cells in shock arena including all time points. p=0.03 (Group) two-way ANOVA, *p=0.024 post-hoc pairwise two-sided Mann-Whitney U-test after Bonferroni correction. **G)** Same as F but for all cells in shock arena. p=0.008 (Time) and p=0.045 (Group) two-way ANOVA. *p=0.012, **p=0.0028, +p=0.072 post-hoc pairwise two-sided Mann-Whitney U-test after Bonferroni correction. **H)** Same as F) but for peri-freeze times only and after randomly downsampling the number of freeze events to match the average number observed during days -2 and -1. +p=0.11 two-way ANOVA (Time). **I)** Same as G) but excluding all peri-freeze times. p=0.0017 two-way ANOVA (Time), *p=0.012, **p=0.01, +p=0.072 post-hoc pairwise two-sided Mann-Whitney U-test after Bonferroni correction. **J)** Mean covariance of freeze-predicting cells detected on Day 1 tracked across time. p=0.01 two-way ANOVA (Time), *p=0.027 post-hoc pairwise two-sided Mann-Whitney U-test after Bonferroni correction. **K-L)** There are no significant differences between the proportion of active units (z-scored) peaks for Control animals compared to the ANI group between 0 and 2 seconds prior to freezing. Line/shading = mean +/- 95% CI. Red: bins with p < 0.05, independent t-test (two-sided).

Figure S7: Reduced activity following anisomycin administration is not an imaging artifact and does not result from global disruption of electrical neural activity in hippocampal neurons.

A-C) Neural activity was tracked across ~5 hours before and after systemic administration of anisomycin. **A)** Cross correlograms for all single and multi-unit activity combined are shown from the pre epoch in a rest box (15 minutes), running on a novel track immediately following anisomycin injection (45 minutes), post epoch in the rest box (3.5 hours), running on a second novel track (45 minutes), and a second post epoch in the rest box (15 minutes). Clear modulation of firing at the theta timescale is observed. **B)** Example trace from electrode in pyramidal cell layer of CA1 showing theta activity 10 minutes and 4 hours 15 minutes post injection anisomycin injection. **C)** Example sharp wave ripple events occurring from 25 minutes to 4 hours 15 minutes post anisomycin injection.

1092 **D-E)** The signal-to-noise ratio of all neurons captured using calcium imaging and active between sessions
1093 was tracked between sessions. **D)** Mean height of calcium transient peaks for all cells matched from day -
1094 1 to 4 hour session. $p>0.63$ both groups, two-sided t-test. **E)** Same as D) but tracking cells from day -1 to
1095 day 1, $p>0.68$ both groups.